(4)

TECHNICAL REPORT BRL-TR-3055

BRL

SPECTRAL STUDIES OF SOLID PROPELLANT COMBUSTION

II. EMISSION AND ABSORPTION RESULTS FOR M-30 AND HMX1 PROPELLANTS

JOHN A. VANDERHOFF

DECEMBER 1989

U.S. ARMY LABORATORY COMMAND

BALLISTIC RESEARCH LABORATORY
ABERDEEN PROVING GROUND, MARYLAND

UNCLASSIFIED

SECURITY CLASSIFICATION OF THIS PAGE

REPORT DOCUMENTATION PAGE

Form Approved OMB No. 0704-0188

1a. REPORT SECURITY CLASSIFICATION: Unclassified	1b. RESTRICTIVE MARKINGS
2a. SECURITY CLASSIFICATION AUTHORITY	3. DISTRIBUTION/AVAILABILITY OF REPORT: Approved for public release; distribution unlimited
2b. DECLASSIFICATION/DOWNGRADING SCHEDULE	
4. PERFORMING ORGANIZATION REPORT NUMBER(S): BRL-TR-3055	5. MONITORING ORGANIZATION REPORT NUMBER(S)
6a. NAME OF PERFORMING ORGANIZATION: US Army Ballistic Research Laboratory; 6b. OFFICE SYMBOL (If applicable): SLCBR-IB	7a. NAME OF MONITORING ORGANIZATION
6c. ADDRESS (City, State, and ZIP Code): Aberdeen Proving Ground, MD 21005-5066	7b. ADDRESS (City, State, and ZIP Code)
8a. NAME OF FUNDING/SPONSORING ORGANIZATION; 8b. OFFICE SYMBOL (If applicable)	9. PROCUREMENT INSTRUMENT IDENTIFICATION NUMBER
8c. ADDRESS (City, State, and ZIP Code)	10. SOURCE OF FUNDING NUMBERS: PROGRAM ELEMENT NO. 61102A; PROJECT NO. AH43; TASK NO.; WORK UNIT ACCESSION NO.

11. TITLE (Include Security Classification)
SPECTRAL STUDIES OF SOLID PROPELLANT COMBUSTION. II. EMISSION AND ABSORPTION RESULTS FOR M-30 AND HMX1 PROPELLANTS

12. PERSONAL AUTHOR(S)
John A. Vanderhoff

13a. TYPE OF REPORT	13b. TIME COVERED	14. DATE OF REPORT (Year, Month, Day)	15. PAGE COUNT
Final	FROM Jun 88 TO Jun 89		

16. SUPPLEMENTARY NOTATION

17. COSATI CODES			18. SUBJECT TERMS (Continue on reverse if necessary and identify by block number)
FIELD	GROUP	SUB-GROUP	
21	02		Combustion, Solid Propellant, Spectroscopy, Absorption, Emission, Concentration, Profiles, SOLID PROPELLANTS

19. ABSTRACT (Continue on reverse if necessary and identify by block number)

A windowed strand burner with a propellant feed mechanism has been used to characterize the steady-state burning of two composite propellants, M-30 and HMX1, at moderate pressure. Both emission and absorption spectroscopy have yielded profile data on three important combustion species: OH, NH, and CN. Relative appearances of these three species are inferred from emission intensity profiles, and absolute concentration profiles are calculated from the absorption data. This is the first absolute determination of these combustion intermediates in a propellant flame. These concentration measurements for OH indicate that the propellant flame temperatures are about 200 K below adiabatic. A maximum value of 40 ppm NH is found for the M-30 propellant flame. Fluctuations in the flame front of HMX1 compromised the determination of maximum concentrations for NH and CN.

20. DISTRIBUTION/AVAILABILITY OF ABSTRACT	21. ABSTRACT SECURITY CLASSIFICATION
☐ UNCLASSIFIED/UNLIMITED ☒ SAME AS RPT. ☐ DTIC USERS	Unclassified

22a. NAME OF RESPONSIBLE INDIVIDUAL	22b. TELEPHONE (Include Area Code)	22c. OFFICE SYMBOL
DR. JOHN A. VANDERHOFF	301-278-7069	SLCBR-IB-I

DD Form 1473, JUN 86 — Previous editions are obsolete. — SECURITY CLASSIFICATION OF THIS PAGE

UNCLASSIFIED

INTENTIONALLY LEFT BLANK.

TABLE OF CONTENTS

INTENTIONALLY LEFT BLANK.

LIST OF FIGURES

LIST OF FIGURES (CONT'D)

LIST OF FIGURES (CONT'D)

INTENTIONALLY LEFT BLANK.

LIST OF TABLES

INTENTIONALLY LEFT BLANK.

I. INTRODUCTION

The detailed chemical steps involved in solid propellant combustion are not well understood; thus probing of the gas phase region close to the burning surface (the reaction zone) can yield essential information for developing a detailed chemistry model. Both emission and absorption spectroscopy are well established non-intrusive probing techniques that can readily be used to identify and profile intermediate combustion products. In this paper the electronic transitions of the combustion diatomic radicals (OH, NH, CN, and CH) are investigated.

The results reported here are an extension of work accomplished previously on the emission and absorption spectroscopy of M-30 propellant combustion.[1,2] A propellant feed mechanism has been incorporated into the windowed strand burner to allow extended data accumulation times for the absorption studies on M-30 and other combusting propellants. In the past, propellant feed mechanisms[3,4] commonly used optical feedback systems to control the propellant position. These feedback systems were, at best, moderately successful depending on the surface burning and gas phase transmission characteristics of the propellant under study. The present configuration incorporates a manual adjustment for establishing a constant feed rate. The present studies also include emission and absorption spectroscopy performed on a nitramine propellant, HMX1. (The HMX1 propellant was provided by T. Edwards, AFAL, Edwards Air Force Base, CA.) Both M-30 and HMX1 are composite propellants; that is, their primary component is crystalline (see Table 1). M-30 is a propellant used for long range artillery and HMX1 is a typical rocket propellant.

Table 1. Propellant Composition

Composition Wt. %	M-30	HMX1
Nitroguanidine	47.7	
Nitrocellulose	28.0	
Nitroglycerin	22.5	
Ethyl Centralite	1.5	
Sodium Aluminum Fluoride	0.3	
HMX		73
TMETN*		17
Polyester Binder**		10
Flame Temperature	2423K @ 1.0 MPa	2617K @ 1.5 MPa

*Trimethylolethanetrinitrate
**Based on polydiethylene glycol adipate

Much has been written concerning the combustion mechanisms of propellants and a survey will not be attempted here; however, a brief generalized sketch of the gas phase chemistry might start with a double base propellant. It is believed that the initial gas phase reactants for double base, nitrocellulose-nitroglycerin (NC/NG) propellants are aldehydes and nitrogen dioxide.[5,6] These reactants then can react in various ways to eventually form final products. At moderate pressures these reactions are delayed by the slow conversion of NO to N_2. Physical evidence for this occurrance comes from the

observation of a dark zone, a region where visible radiation is absent. This region is located between the burning surface and the visible flame. It decreases in extent as the pressure is increased. M-30, on the other hand, has a much smaller or no dark zone. An obvious difference between M-30 and a double base propellant is the large amount of nitroguanidine present in M-30 (see Table 1). Nitroguanidine combustion may provide NH_x species which can enhance the conversion of NO to N_2.[7] Detailed profiles of these species in conjunction with a chemical model may be able to explain this observation. Nitramine propellant combustion is also thought to occur with aldehydes and nitrogen dioxide as initial gas phase reactants. Hydrogen cyanide and nitrous oxide are also included as initial reactants.[5,8] Depending upon the composition of the nitramine propellant dark zones may or may not be produced at moderate pressure. Detailed chemical models have been produced to describe both neat HMX[9] and RDX[10,11] combustion. For the RDX case there is some recent experimental data[12] for comparison. The model shows a good agreement with the data and indicates that the principal reaction in the flame zone of RDX burning at 0.05 MPa is the oxidation of hydrogen cyanide with nitric oxide. These types of models produce species and temperature profiles for the gas phase propellant chemistry. Part of the research goal here is to be able to obtain profile data of species active in the combustion process for comparison with and validation of these models.

II. BACKGROUND

Solid propellant combustion chemistry has been studied for many years and the review articles by Fifer,[5] Lengelle,[6] and Kubota[8] well describe many of the important contributions. As a background for the present study the experimental references will be primarily to investigators that have employed uv-visible spectroscopic techniques. Homogeneous double base propellants have been studied with emission and absorption techniques.[13-15] In these studies, black body temperature estimates, line emission signals from impurity metallic species and a C_2 radical species were reported for the final flame zone (explosion zone). Heterogeneous composite propellants where the oxidizer is ammonium perchlorate (AP) or a nitramine (HMX-cyclotetramethylenetetranitramine, and RDX-cyclotrimethylenetrinitramine) have been studied more extensively in the recent past. Emission intensity profiles of several chemically active transient species have been obtained for AP and nitramine propellants. CN[15-19] and OH[18,19] profiles were measured for both types of propellants, whereas an NH profile is published only for a nitramine propellant.[15,19] A composite propellant, M-30, which is also referred to as atriple base propellant, has recently been investigated with emission spectroscopy[1] and emission intensity profiles for NH, CN, and OH were reported. These emission studies may not give a true representation of the species concentration; that is, complete equilibrium may not be achieved during combustion, hence the excited state species which emit visible/uv radiation are not necessarily equilibrated with respect to the partitioning of energy in their electronic, vibrational, and rotational energy levels. Nonetheless, there is such a scarcity of data obtained for actual propellant combustion conditions (absolute concentrations are virtually non-existent) that emission studies provide much of the experimental data base on transient species. A number of laser based techniques which optically probe the region of interest have a potential for determining absolute concentrations. Laser induced fluorescence (LIF) measurements have been published which illustrate fluorescence intensity profiles of CN,[15,20] NH,[20] and OH,[15,20] and NO_2[21] in

nitramine propellant combustion. In nitramine propellant combustion a gas phase temperature profile has been determined from probes of the rotational structure of OH with LIF.[21] Coherent anti-Stokes Raman scattering (CARS) has been applied to a nitramine propellant burning in room air.[22] Recently CARS has been used to probe a nitramine propellant burning at 2.3 MPa in a helium environment.[23] Simultaneous spectral signatures for HCN, CO, N_2, and H_2 were obtained as a function of distance from the propellant surface. Here temperatures, as well as absolute concentrations of CO, H_2, and N_2, have been determined.

III. EXPERIMENTAL

A windowed strand burner and the optical paths for both emission spectroscopy and video recordings are shown on Figure 1. Since these measurements have been discussed previously,[1,2] only a brief description will be given here. The camera system provides a real time display and a video recording of the propellant burn. This video information can be used to trigger other parts of the experiment, determine propellant burn rates, and roughly assess the degree of flatness for the burn. A magnification of nine by the macro lens allows verification of whether the propellant burns in a cigarette fashion with a horizontal, flat burning surface. The degree of flatness can be visually assessed to within 0.15 mm. Neutral density filters and aperture control allow adjustment for the substantial variation in brightness for different propellants. Emission signals from the propellant sample are generally collected and focussed onto a 0.1 mm horizontally oriented entrance slit by two convex lenses having a magnification of two. The resulting spatial resolution is nominally 0.1 mm full width at half maximum (FWHM). This resolution has been experimentally verified by recording the signal produced from various size illuminated slits as a function of position. However, when a propellant is combusting near its deflagration limit in pressure there can be variations in emission intensity as well as movement of the flame front. This behavior degrades the spatial resolution. Various monochromators have been used to disperse the emission signal onto an intensified linear photodiode array (Reticon) and a computer is used for acquisition, manipulation, and storage of the optical data. Depending on circumstance, spectral resolution has varied from 0.03 to 0.3 nm.

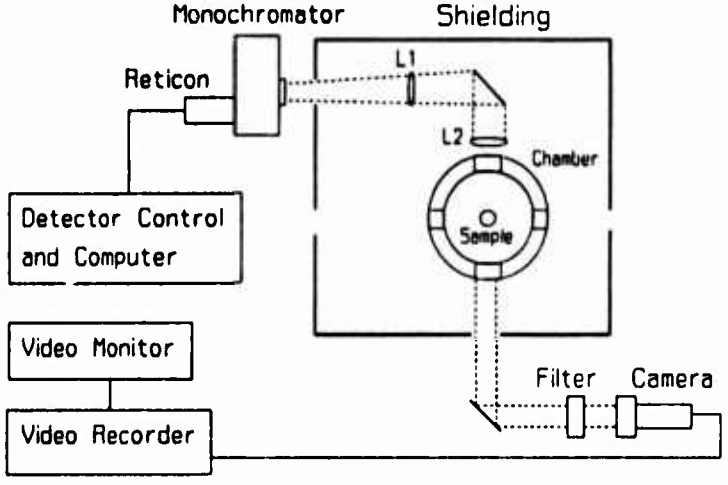

Figure 1. Top View of Strand Burner and Associated Optical Systems

Light produced from 1000 Watt Xenon or Xenon-mercury arc lamps was used for the absorption studies. The optical path is shown on Figure 2. Two 20 cm convex lenses focus and recollimate the light beam and two apertures and a 0.15 mm pinhole confine the spatial resolution to approximately 0.15 mm in the burning direction. A 10 cm focal length cylindrical lens line focusses the light on a spectrometer entrance slit. The aperture between the propellant strand and the monochromator minimizes the collection of the emission signal. Aperture sizes between 0.5 and 1.0 mm were used to keep the emission signal levels to values such that errors in the absorption measurement would be less than 2% from this effect. For these absorption studies, a 0.3 m spectrometer with 2400 grooves per mm grating was operated both in first and second order giving a spectral resolution of 0.033 or 0.066 nm. This resolution accommodates a 6 nm band of light to be sampled at one time with the intensified photodiode array. Absorptions of interest are much narrower than this 6 nm band; thus, both intensities of wavelengths which undergo absorption (I) and which do not (I_o, at a slightly different wavelength) can be recorded simultaneously.

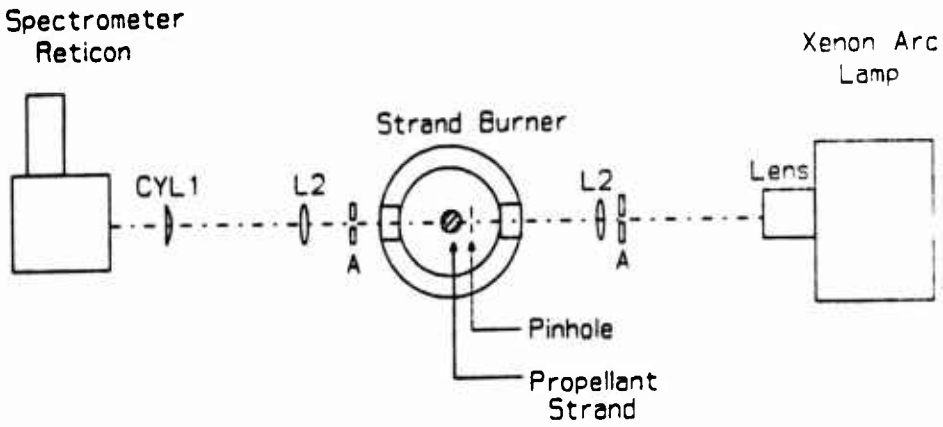

Figure 2. Optical Path for Absorption Experiments

Previously, emission[1] and absorption[2] experiments were conducted while the propellant burned through the sampling region. With this arrangement, data of marginal quality were collected for OH absorption in M-30 propellant. Increasing the time to collect data, hopefully improving its quality, has been realized with the incorporation of a propellant feed mechanism in the windowed strand burner. A sketch of this feed mechanism is shown on Figure 3. The mechanism is more rudimentary than previous feed mechanisms[3,4] in several respects. First, the feed mechanism is not enclosed in the pressure vessel, but rather couples in linear motion by a drive shaft sealed with a plastic ferrule swage. Second, the drive shaft is unidirectional during the experiment and the rate at which it moves is preset with a calibrated potentiometer rather than maintaining control with an optical feedback system. The rate at which the drive shaft moves is set to be some fraction of the burn rate of the propellant. For the experiments reported here this rate was typically 75% of the propellant burn rate which results in a factor of four increase in data acquisition time.

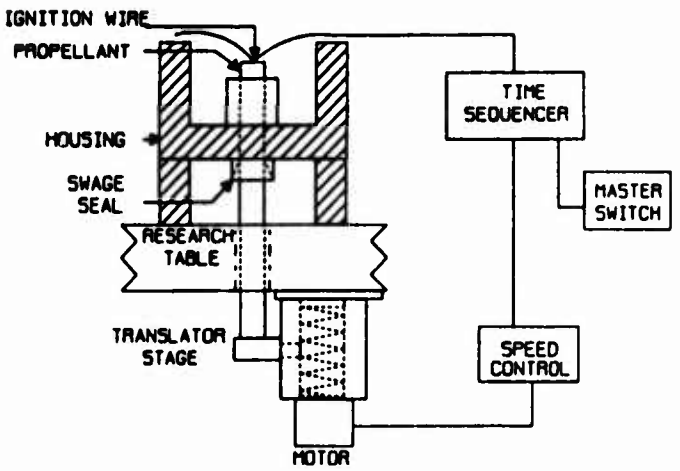

Figure 3. Propellant Feed Mechanism and Ignition Diagram

The following sequence of events would occur for a typical experimental run. After installing the propellant sample and connecting the ignition wire, the strand burner is closed and pressurized. Next, the video recording system is turned on and propellant burning is initiated by engaging the master switch. This master switch starts a time sequencer which turns on a power supply to heat the ignition wire. For the propellant feed experiments, the time sequencer also starts the propellant feed mechanism after a predetermined time delay. This time delay is normally used to also trigger the photodiode array which repetitively scans and resets many times while storing each of these scans into buffer memory. The total data accumulation time, as well as the time for each scan, can be varied over a wide range. Typical scan times ranged from 16 to 50 ms and total data accumulation times were major fractions of the propellant sample burn times (5 to 15 s). For each scan time (50 ms maximum), the burning propellant surface moves a negligible amount, about .025 mm.

Two types of composite propellants have been experimentally studied and their composition and flame temperature are given in Table 1. These adiabatic flame temperatures were calculated for constant pressure conditions using the NASA-Lewis thermochemical equilibrium code.[24] Nitroguanidine is the main ingredient in M-30 and it is crystalline. The crystals are rod like with diameters about 0.007 mm and length to diameter ratios of about 20. Ethyl centralite is a long term stabilizer and sodium aluminum fluoride is a muzzle flash suppressant. HMX is the main ingredient in HMX1 propellant and it is crystalline consisting of a mixture of particles 20 μm in diameter and 200 μm in diameter. TMETN is an energetic plasticizer and the polyester binder is inert. A methane/nitrous oxide premixed flame has been used extensively in this experimental work because, from previous experience,[25] it was known that this flame could readily provide high quality steady state spectra and rough signal strengths for the combustion species to be investigated in the transient experiments on propellant samples. This premixed flame was supported on a small burner; a top view is shown on Figure 4a. A burner with a head diameter of 0.4 cm was chosen so that it would be similar to the absorption path lengths of the propellant samples (see Figures 4b and 4c). Long pathlengths are traditionally desirable for trace species since for small

absorptions the absorption increases proportionally with pathlength. However, in these studies, the overriding concern was to produce a horizontal burning surface; i.e., a surface which is parallel to the direction of the arc lamp light beam. Three propellant geometries have been investigated: cylinders, rectangular bars, and eight-sided bars. Small diameter (0.55 cm) M-30 propellant cylinders readily burned cigarette fashion with a horizontal surface as long as the ignition point was the center of the cylinder; see Figure 5a. Difficulties were encountered when burning 1.25 cm diameter M-30 propellant cylinders. Here, non-horizontal burning frequently occurred and thus, these larger samples were not further studied. Problems were also encountered when burning the square cross section (0.65 cm on a side) bars of HMX1 propellant. The problem is visually depicted on Figure 5b where it is shown that the corners of the propellant are not at the same level as the center portion. Cutting the HMX1 propellant bar to produce an eight sided cross section, shown on Figure 4d, minimized this problem, which is believed to be due to edge cooling, but it also created another problem. Up to this point, an inert gas flow around the propellant[1] had been sufficient to maintain a cigarette fashion propellant burn (i.e., no coating of the sides with an inhibitor). Now, this freshly cut eight-sided HMX1 propellant strand burned down the side a substantial fraction of the time because of ignited surface particles fall down the sides of the propellant sample creating further ignition points. This problem has been removed by thinly coating the sides of these freshly cut samples with fingernail polish inhibitor.

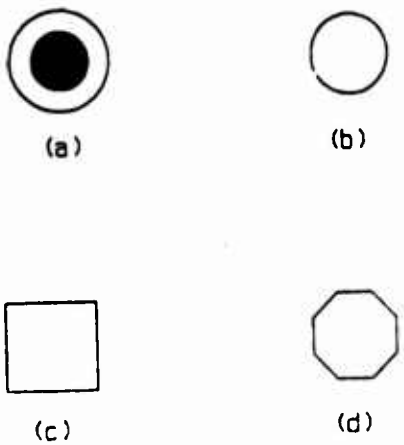

Figure 4. Absorption Path Lengths for the Various Combustion Systems Studied. (a) The hatched area represents a 0.4 cm diameter for the small CH_4/N_2O burner. (b) A diameter of 0.55 cm for the cylindrical sticks of M-30 propellant. (c,d) A path length of 0.65 cm for HMX1 propellant.

IV. DATA ANALYSIS

In this section, working equations are written down which can be used to extract temperatures and absolute concentrations from experimental emission and absorption spectra. Development and detailed discussions of these equations can be found elsewhere.[26-30]

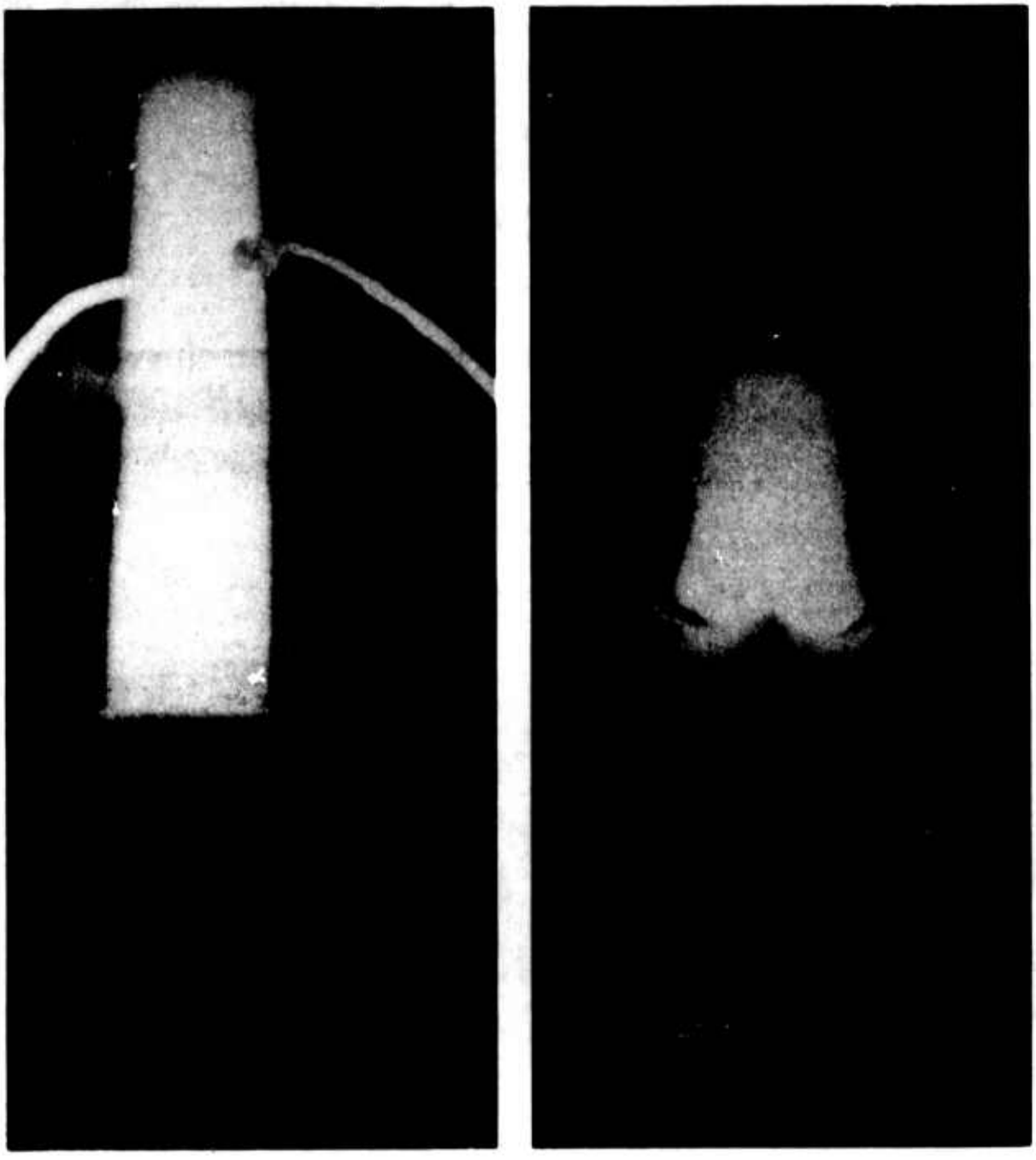

Figure 5. (a) Photograph of M-30 Burning in 1.0 MPa Nitrogen.
(b) Photograph of HMX1 Burning in 1.5 MPa Nitrogen.

Assuming a Boltzmann distribution, vibrational and rotational temperatures of an excited molecular state can be computed from measured emission intensities. The intensity of a spectral line in emission is given by

$$I_{em} = C_1 \, S_{J'J''} \, q_{v'v''} \, \nu^4_{J'J''} \exp\left[-\frac{hc}{k}\left(\frac{F_{J'}}{T_{R'}} + \frac{G_{v'}}{T_{v'}}\right)\right] \quad , \tag{1}$$

where single and double prime refer to the upper and lower states, respectively. J and v are rotational and vibrational quantum numbers, respectively. C_1 is a constant, $S_{J'J''}$ is the rotational line strength, $q_{v'v''}$ is the Franck-Condon factor, $\nu_{J'J''}$ is the transition frequency and F and G are the term values for rotation and vibration, respectively. In this paper the vibrational temperatures ($T_{v'}$) have been calculated from the experimental data when the rotational contribution can be accounted for by a vibrational bandhead. The rotational temperatures ($T_{R'}$) are obtained by working within the v'=v"=0 transition. Both $T_{V'}$ and $T_{R'}$ could, with more extensive computations, be obtained from a single emission spectrum that covered several vibrational bands.

Rotational temperatures for the molecular ground state ($T_{R''}$) can be determined from experimental absorption spectra and these spectra are more likely to be described by a Boltzmann distribution than emission spectra. The intensity of a spectral absorption line is given by

$$I_{abs} = C_2 \, S_{J''J'} \, q_{v''v'} \, \nu_{J''J'} \exp\left[-\frac{hc}{k}\left(\frac{F_{J''}}{T_{R''}} + \frac{G_{v''}}{T_{v''}}\right)\right] \tag{2}$$

where C_2 is a constant. A plot of $\ln (I_{abs}/S_{J''J'}\nu_{J''J'}C_2)$ versus $F_{J''}$ for various rotational transitions will produce a straight line of slope $- hc/kT_{R''}$ from which the rotational temperature is determined. In the results section, temperatures are calculated from both emission and absorption spectra of the OH molecule, and for these calculations, the effective rotational line strengths used were obtained from the Einstein B coefficients reported by Dimpfl and Kinsey[31] (see Eq. 6) which includes a J dependence of the excited state lifetime, and hence, electronic transition strength.

Absolute concentrations can be determined from absorption spectra provided the temperature and certain molecular data are known. The peak fractional absorption can be expressed as[27,28]

$$\left[\frac{I_o - I}{I_o}\right]_{peak} = \frac{L}{\Delta\nu} \int_{line} k_\nu \, d\nu \tag{3}$$

when the absorption is weak and the light source bandwidth is larger than the absorption line. I_o is the initial light source intensity before passing through the sample region and I is the transmitted intensity. L is the path length for absorption, $\Delta\nu$ is the spectral bandwidth, and k_ν is the absorption coefficient. In terms of the molecular parameters, the peak fractional absorption for a transition originating from a ground vibrational state is written as

$$\left[\frac{I_o - I}{I_o}\right]_{peak} = \frac{N_T L h}{Q_T \alpha \Delta\nu} \nu_{J''J'} B_{J''J'} (2J''+1) \exp\left[-\frac{hc}{kT_{R''}} (G(0) + F_{J''})\right] \quad (4)$$

where N_T is the total concentration of a particular molecule, Q_T is the partition function, and $B_{J''J'}$ are the Einstein coefficients of absorption (with units appropriate for radiation density). As stated earlier, the Einstein coefficients for OH came from Dimpfl and Kinsey[31] and the transition frequencies for OH were obtained from Dieke and Crosswhite.[32] Most often these B-coefficients must be generated from published experimental radiative lifetimes (T) for various molecules. The Einstein A coefficient for spontaneous emission is related to the lifetime as

$$A_{J'J''} = \frac{1}{T}\left[(2S+1)\, g_{e'}\, q_{v''v'} \frac{S_{J''J'}}{\sum_{J''} S_{J''J'}}\right] \quad (5)$$

where 2S+1 is the multiplicity of the state and $g_{e'}$ is the degeneracy of the upper electronic state. The B coefficients are related to the A coefficients by

$$B_{J''J'} = \frac{1}{8\pi h \nu^3_{J''J'}} \left(\frac{2J'+1}{2J''+1}\right) A_{J'J''} \quad . \quad (6)$$

B-coefficients for NH and CN were generated in this manner for use in Eq. 4. The molecular parameters from Huber and Herzberg[26] employed for determining the temperatures and concentrations are given in Table 2. The Franck-Condon factors and radiative lifetimes for NH[33,34] and CN[35,36] are also included in Table 2.

Table 2. Molecule Specific Parameters

Species	NH		OH		CN	
State	$A^3\Pi$	$X^3\Sigma^-$	$A^2\Sigma^+$	$X^2\Pi$	$B^2\Sigma$	$X^2\Sigma^+$
α_e (cm^{-1})	0.745	0.649	0.786	0.724	0.023	0.017
B_e (cm^{-1})	16.675	16.699	17.358	18.910	1.973	1.900
ω_e (cm^{-1})	3231.2	3282.2	3178.8	3737.8	2163.9	2068.6
$\omega_e x_e$ (cm^{-1})	98.6	78.3	92.9	84.9	20.2	13.1
q_{00}		0.945				0.9086
q_{11}		0.936				0.7568
T (ns)	418				60.7	

V. RESULTS

A. Video

Generally, the experimental data reported here have been collected in a temporal fashion and subsequently converted to a distance from the propellant surface. The necessary conversion information is a burn rate which can be

determined from video recordings. Burn rates for the two propellants under study have been obtained as a function of nitrogen pressure and are displayed on Figure 6.

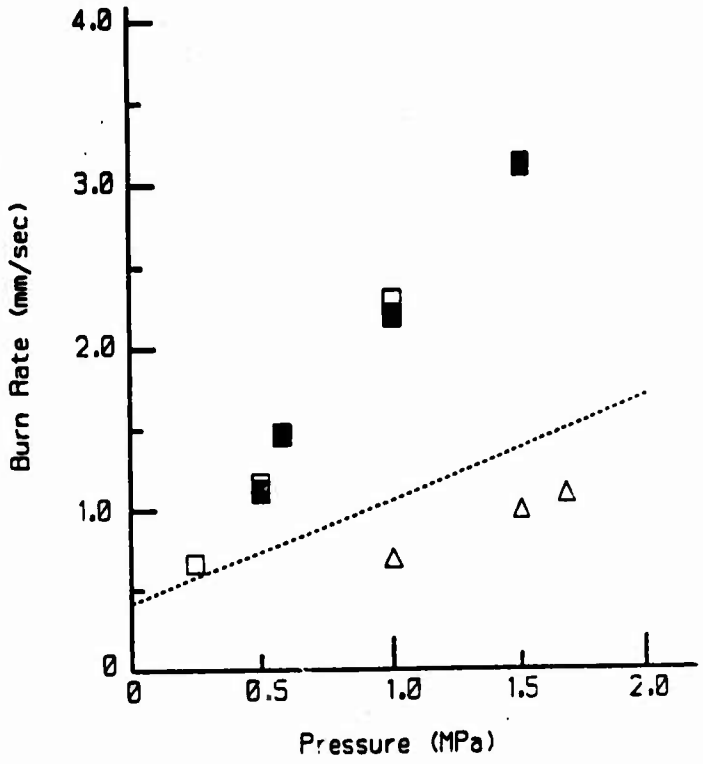

Figure 6. A Comparison of Burn Rate Measurements as a Function of Nitrogen Pressure for M-30 and HMX1 Propellants. M-30 propellant (present data (■), Miller (□)). HMX1 propellant (present data (Δ), Edwards (----)).

The present data (■) for M-30 propellant are in excellent agreement with Miller's data[37] (□). For HMX1, the present data (Δ) are about 30% less than an average of measurements (----) made by Edwards.[15] These data demonstrate that M-30 burns substantially faster than HMX1 over this pressure range. The video system provides other information as well. For example, visible broad band emission was about five times larger for M-30 than for HMX1 as determined from the amount of neutral density filtering placed in front of the video camera. Larger amounts of sodium in M-30 may be responsible for this behavior. Nonetheless, these results show, in most cases, the best signal to noise ratio data for both emission and absorption is from the HMX1 propellant samples. The nitrogen pressures and propellant geometries for which these experiments were conducted are close to the lower limit for ignition and self sustained burning. These limits are approximately 0.3 MPa for M-30 and 0.4 MPa for HMX1. Consequently, it was not altogether surprising that the video recordings indicated non-steady burning for HMX1. Initially the plan was to record HMX1 data at 1.0 MPa since most of the M-30 data was for that pressure. However, a nitrogen pressure of 1.5 MPa was required to reduce the cyclic attaching and lifting off of the HMX1 luminous flame. No photographic

indications of a dark zone were apparent for M-30 burning in 1.0 MPa nitrogen. The non-steady burning behavior of HMX1 rendered the video data ambiguous for evidence of a small dark zone.

B. Emission

Emission intensity studies for electronic transitions in NH, OH, and CN have been previously reported for M-30 propellant.[1] Here, emission signals for HMX1 propellant were large enough to allow simultaneous recording of NH, OH, and CN on the photodiode array detector. These emission intensities as a function of wavelength for a CH_4/N_2O flame are displayed on Figure 7 where the transition regions are 309 nm for OH ($A^2\Sigma^+ \rightarrow X^2\Pi$ (0,0)), 336 nm for NH ($A^3\Pi - X^3\Sigma^-$ (0,0)), and 359 nm for CN ($B^2\Sigma^+ - X^2\Sigma^+$ (1,0)). Emission intensities of NH, OH, and CN as a function of distance from the HMX1 propellant surface are shown on Figure 8. These intensities are determined from multiple emission spectra (similar to Figure 7) taken at specified time intervals where this time has been transformed to distance via the burn rate measurement. The exact zero position for the propellant surface is somewhat arbitrary (estimated as ±0.3 mm) due to the spatial resolution of the optical system, flatness of the burning surface, and the unsteady nature of the flame front. However, the relative positions of the NH, CN, and OH intensity profiles should be quite good since these data were obtained simultaneously for each propellant sample. A simple analysis of the data in Figure 8, as well as data for a lower and a higher nitrogen pressure (not shown), point out that the NH and CN emission intensities peak at the same distance from the propellant surface (~0.6 mm) and that this position moves closer to the propellant surface with increasing pressure. The emission intensity for OH peaks about 1 mm further from the propellant surface than either NH or CN and extends to much greater distances from the propellant surface. This type of behavior is found in many premixed laminar flames. The fluctuations for the OH emission intensity, shown on Figure 8, are not due to signal-to-noise problems, but rather due to fluctuations of the flame front on the burning propellant surface. Evidence for a fluctuating flame front correlating with OH emission comes from the video record for the propellant burn.

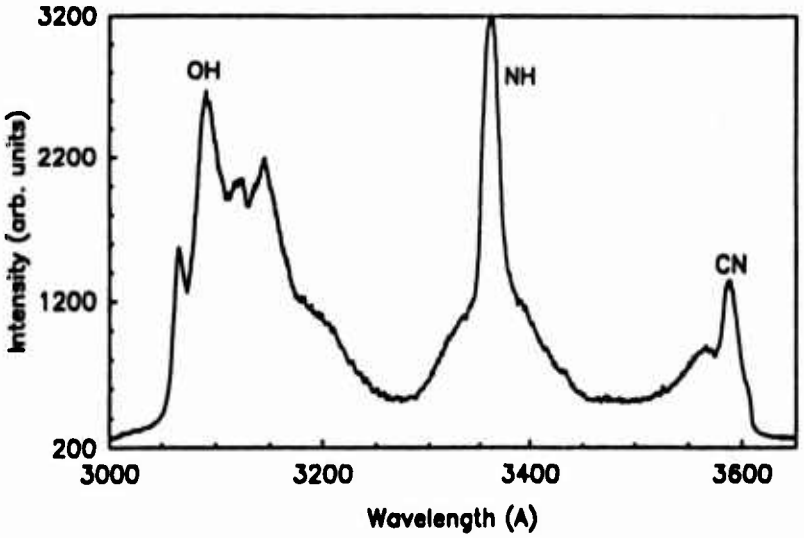

Figure 7. Emission Intensity as a Function of Wavelength for a CH_4/N_2O Flame. The features around 3100A are from OH. NH appears at 3360A and CN at 3590A.

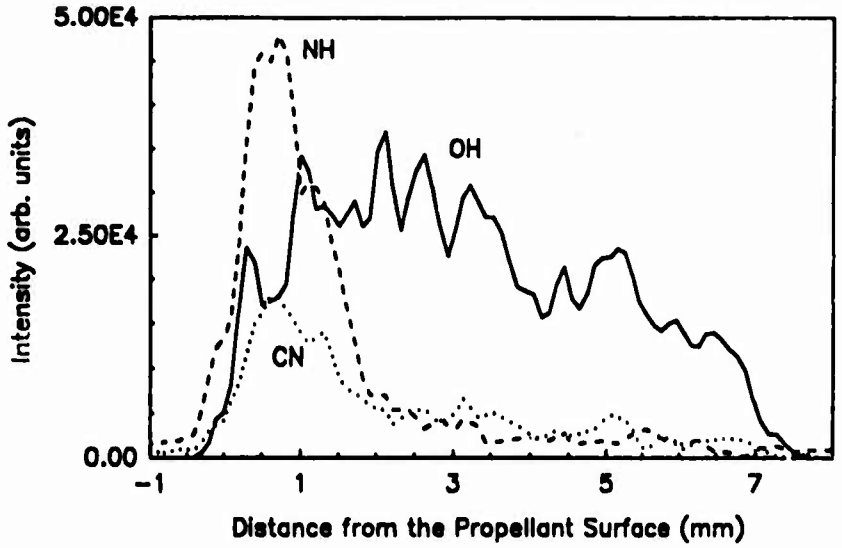

Figure 8. Emission Intensity Profiles as a Function of Distance from the Propellant Surface for HMX1 Burning in 1.5 MPa Nitrogen. The solid line is OH, the dotted line CN, and the dashed line NH.

Analogous to several other investigations,[15,21] negative results were obtained in the present study when looking for evidence of the formation of CH in M-30 and HMX1 propellant flames. Light emission from the $A^2\Delta - X^2\Pi$ system of CH is a structured signature that can uniquely identify the CH molecule. An example spectrum obtained from a CH_4/N_2O flame is shown on Figure 9 where the (0,0) and (2,2) Q heads are at 4314 and 4324Å, respectively. No signals of this nature were observed during the emission experiments on M-30 burning in 1.0 MPa nitrogen and HMX1 burning in 1.5 MPa nitrogen. In order to somewhat quantify these observations on CH, absorption measurements were also conducted. No evidence of absorption was observed in a CH_4/N_2O flame and an upper limit of 0.2% was placed on the absorption. By analogy with CH concentration measurements made by Eckbreth, et al.,[27] an upper limit for CH concentration in the CH_4/N_2O flame was determined to be 30 ppm. No CH absorption could be identified in the combustion of either M-30 or HMX1 and the upper limit for CH concentration is also 30 ppm.

C_2 is another transient diatomic species whose light emission from the $d^3\Pi_g - a^3\Pi_u$ Swan system can readily be observed in a CH_4/N_2O flame. During the propellant studies, emissions of C_2 were not observed and this result is consistent with the observations of Edwards.[15] No attempts have been made to quantify these observations.

In propellant combustion diagnostics, one of the most important fundamental parameters to measure is the temperature profile. These profiles are generally measured with fine wire thermocouples so that detailed temperature information is obtained in both the solid and gas phase. Unfortunately, part of the gas phase cannot usually be measured since most thermocouples burn out at temperatures substantially below the final flame temperature. Both emission and absorption spectroscopy contain information from which temperatures can be calculated. Emission spectroscopy can provide

excited electronic state temperatures for both vibrational and rotational states (see Eq. 1). These temperatures, however, are only representative of the gas temperature if there is thermal equilibrium in the excited state. An example that demonstrates an excited state temperature much higher than the gas temperature is found in the CH_4/N_2O flame. An emission spectrum of the CN violet system ($B^2\Sigma^+ - X^2\Sigma^+$, $\Delta v = 0$) is shown on Figure 10. The ratio of the bandhead intensities for the different vibrational bands give temperatures of ~4200 K for the (1,1)/(0,0) ratio and ~5300 K for the (2,2)/(0,0) ratio. These values are almost double the adiabatic flame temperature, and thus most certainly do not represent a true gas temperature. Other investigators[38] have observed similar behavior of CN* for various flame systems, including CH_4/N_2O.[15] The results of their studies indicate that the chemiluminescent reaction

$$C_2^* + NO \rightarrow CN^* + CO \qquad (7)$$

is responsible for producing excited CN. Moreover they find that increasing NO concentrations reduce CH* and C_2* emission while CN* and NH* increase. These observations have a bearing on the differences seen in the emission spectra of the CH_4/N_2O flame and the two propellants investigated. Not much NO is produced in the CH_4/N_2O flame and consequently CH* and C_2* emission is observed. However, NO_2 is the main oxidizer for the propellant flames studied. NO_2 is converted readily to NO which could explain the observance of CN* and NH*, but not C_2* and CH* in these propellants.

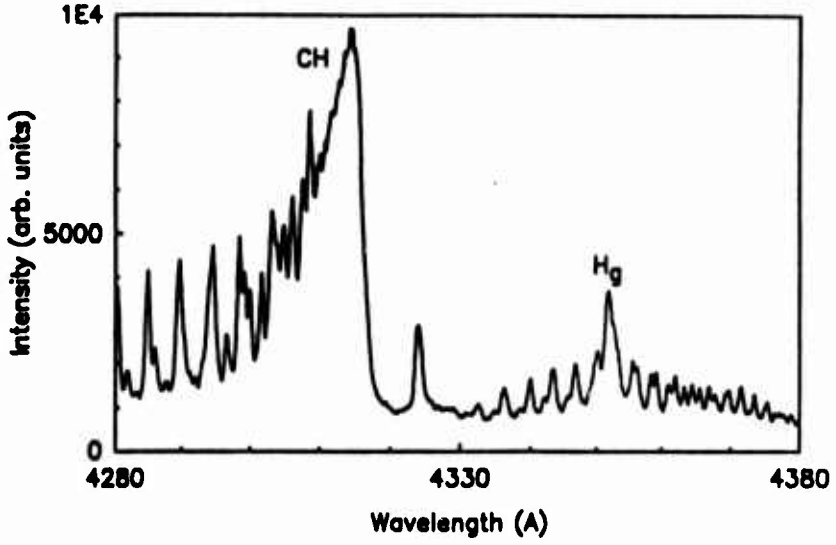

Figure 9. Emission Intensity as a Function of Wavelength for a CH_4/N_2O Flame. The (0,0) bandhead for CH at 4314A is the most prominent feature.

*Molecule in an excited electronic state.

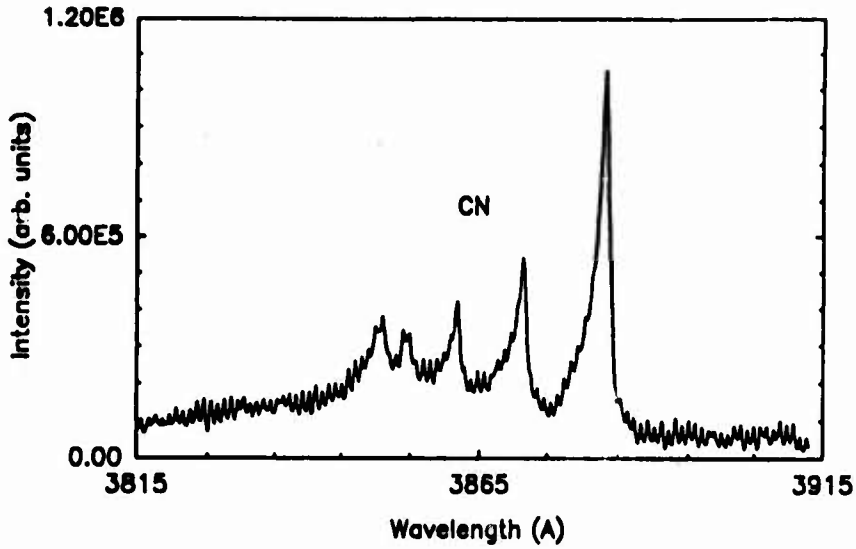

Figure 10. Emission Intensity as a Function of Wavelength for CN in a CH_4/N_2O Flame. The $\Delta v=0$ progression for the violet system is displayed.

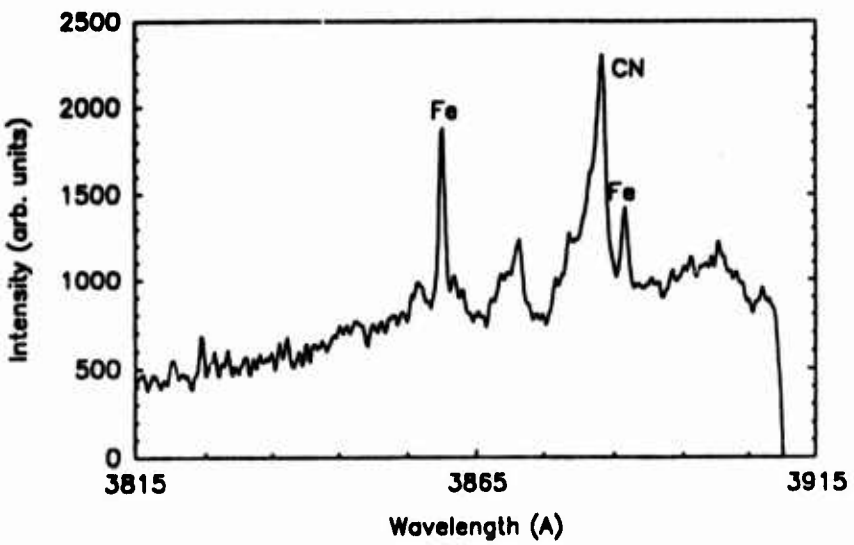

Figure 11. Emission Intensity as a Function of Wavelength for CN in M-30 Burning in 0.66 MPa Nitrogen. Line-like features at 3860 and 3886A are probably due to an iron impurity.

A CN violet system emission spectrum from M-30 burning in .66 MPa N_2 is shown on Figure 11. Line like features at 3860 and 3886A are believed due to an iron impurity. A temperature of 3000 K is calculated from the (1,1)/(0,0) emission intensity ratio and this is again about 600 K higher than a constant pressure thermochemical equilibrium temperature calculation. Thus, there is evidence of the excited state production of CN, but the temperatures are not nearly as far from thermal equilibrium as in the CH_4/N_2O case. Many factors could account for this difference. An obvious difference is the possibility

of collisional relaxation coming from pressure. An emission spectrum of CN taken for HMX1 burning in 1.0 MPa nitrogen is shown on Figure 12. Also displayed for comparison is an emission spectrum of a CH_4/N_2O flame burning in room air. The wavelength region from 4150 to 4216Å encompasses the CN violet system $\Delta v = -1$ region, where $\Delta v = v'-v''$. A ratio of the bandhead vibrational intensities indicates a temperature of T_v, = 2800 K for HMX1 and a temperature again in excess of 4500 K for the CH_4/N_2O flame. The thermochemical equilibrium temperature for HMX1 is about 200 K below that computed from the CN spectrum in Figure 12, and this difference is within the error of the experiment. These data supply some evidence that CN is thermally equilibriated for these specific measurement conditions. However, this data should not be used on a stand alone basis for gas temperature. Other features shown on Figure 12 include a calcium impurity peak at 4226Å in the HMX1 spectrum, as well as spectral evidence for the presence of CH in the CH_4/N_2O flame and no evidence for the presence of CH in the HMX1 flame.

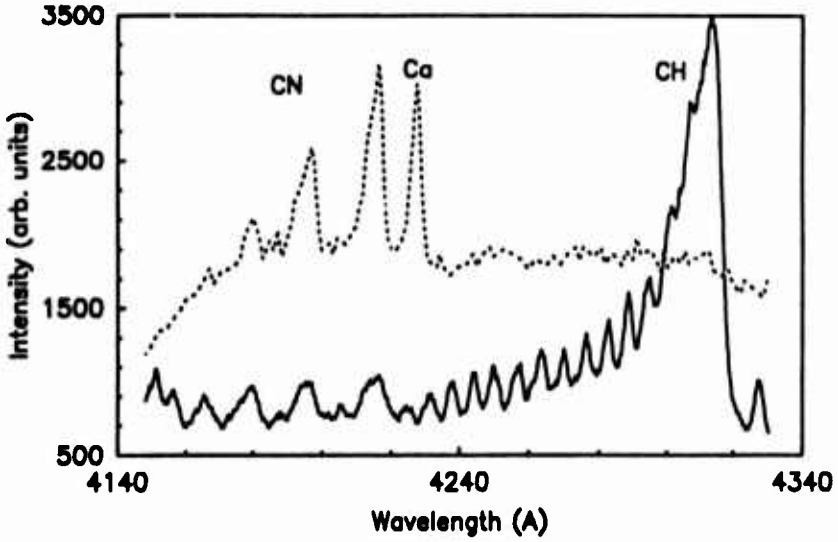

Figure 12. Emission Intensity as a Function of Wavelength Over CH and CN Emitting Regions. The solid line is for a CH_4/N_2O flame, while the dashed line represents emission from HMX1 burning in 1.0 MPa nitrogen. The wavelength region from 4150 to 4216Å encompasses the $\Delta v=1$ violet system of CN and the (0,0) Q bandhead for CH can readily be observed at 4314Å.

The 3360Å system of NH ($A^3\Pi - X^3\Sigma^-$, $\Delta v=0$) can be readily observed in emission and example spectra for the atmospheric pressure CH_4/N_2O flame, HMX1 burning in 1.5 MPa nitrogen and M-30 burning in 0.66 MPa nitrogen are shown on Figures 13, 14, and 15, respectively. A temperature T_v, again can be calculated from the ratio of the bandheads. These values are 2350 K for the CH_4/N_2O flame, 2100 K for HMX1, and 2200 K for M-30. The CH_4/N_2O flame temperature obtained in this manner is in excellent agreement with the temperatures derived from rotational ground state spectral data on OH (to be discussed). Temperature values for the propellant flames are lower than the adiabatic equilibrium temperatures, but this may be due in large part to the experimental uncertainty involved with the smallness of the (1,1) bandhead signal at 3370Å.

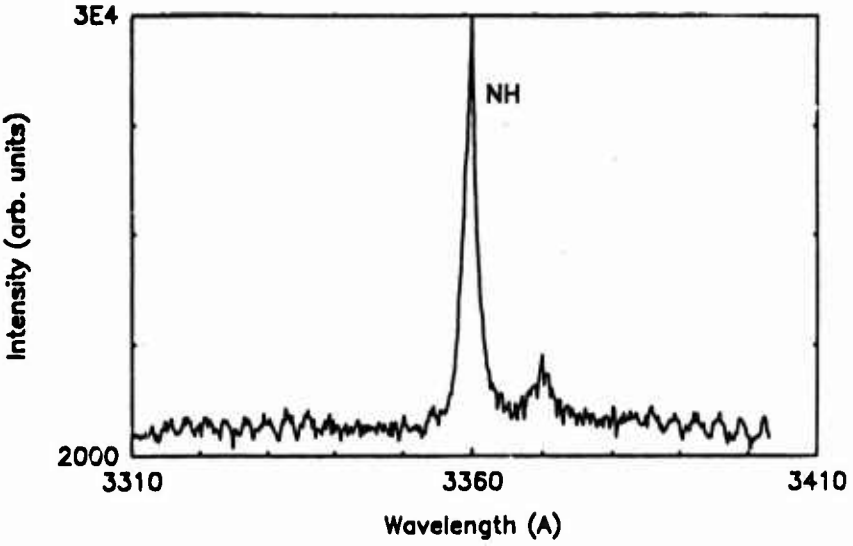

Figure 13. Emission Intensity as a Function of Wavelength for NH in a CH_4/N_2O Flame

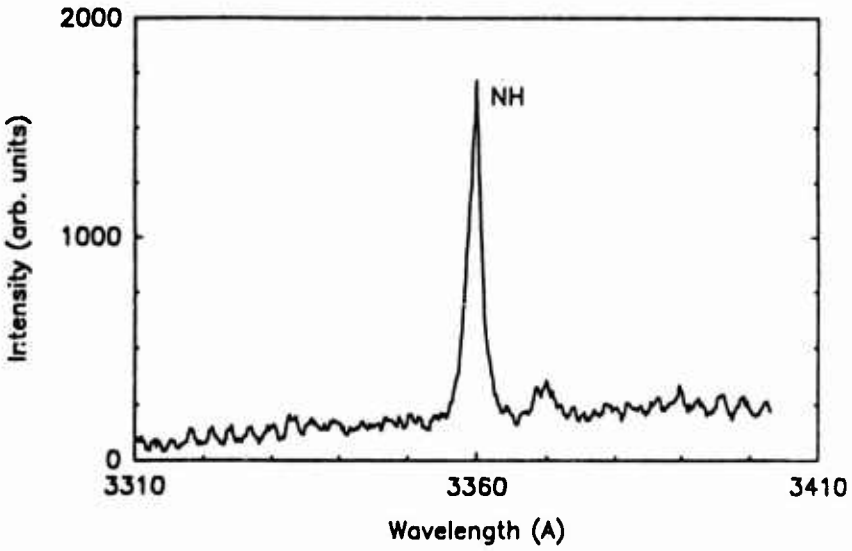

Figure 14. Emission Intensity as a Function of Wavelength for NH in HMX1 Burning in 1.5 MPa Nitrogen

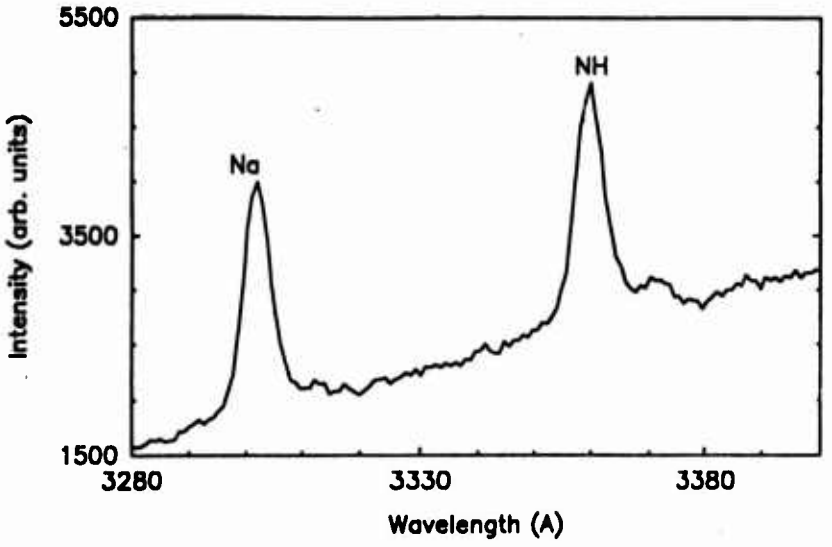

Figure 15. Emission Intensity as a Function of Wavelength for NH in M-30 Burning in 0.66 MPa Nitrogen. The feature at 3302Å is from sodium.

Under moderate resolution (0.3Å) some well resolved rotational lines can be observed for the 3064Å system ($A^2\Sigma^+ - X^2\Pi$, $\Delta v=0$) of the OH molecule. Example emission spectra for a CH_4/N_2O flame and HMX1 burning in 1.5 MPa nitrogen are displayed on Figures 16 and 17, respectively. The signal-to-noise ratio for OH emission in M-30 was very poor and thus a representative spectrum is not shown. Emission intensity data of Figure 16 were used to generate Figure 18 where the ln ($I_{em}/S_{J',J''}\nu^4 C_1$) versus $F_{J'}$ is plotted yielding a temperature ($T_{R'}$) of 2360 K ±130 K for the CH_4/N_2O flame. The six isolated OH lines used for temperature determinations for both emission and absorption are given in Table 3. Unfortunately, the OH signal from the HMX1 propellant was not sufficient for a well enough resolved spectrum to perform a similar temperature analysis (Figure 17). It should be mentioned here that with either moderate improvement in signal detection or a mildly elaborate fitting program, it would be possible to perform temperature determinations on burning HMX1 from OH emission spectra.

Table 3. OH Rotational Transitions for Computing Temperatures from Absorption and Emission Boltzmann Plots

Transition	Energy (cm^{-1})	Wavelength (A)
$R_2(3)$	289.1	3077.03
$Q_1(4)$	355.5	3083.28
$Q_1(5)$	544.1	3085.20
$Q_1(6)$	768.1	3087.34
$Q_2(7)$	1077.1	3094.62
$O_1(9)$	1652.3	3095.34

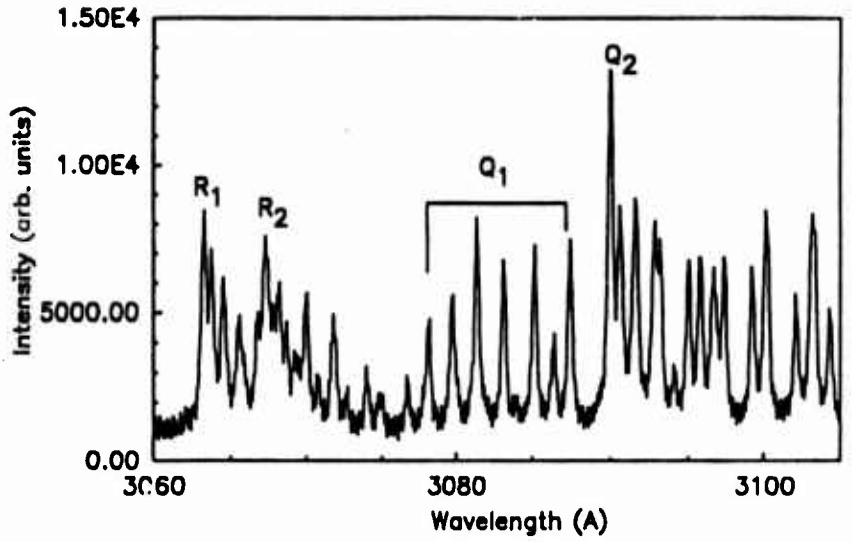

Figure 16. Emission Intensity as a Function of Wavelength for OH in a CH_4/N_2O Flame. The Q_1 branch structure between 3075 and 3087A is well resolved.

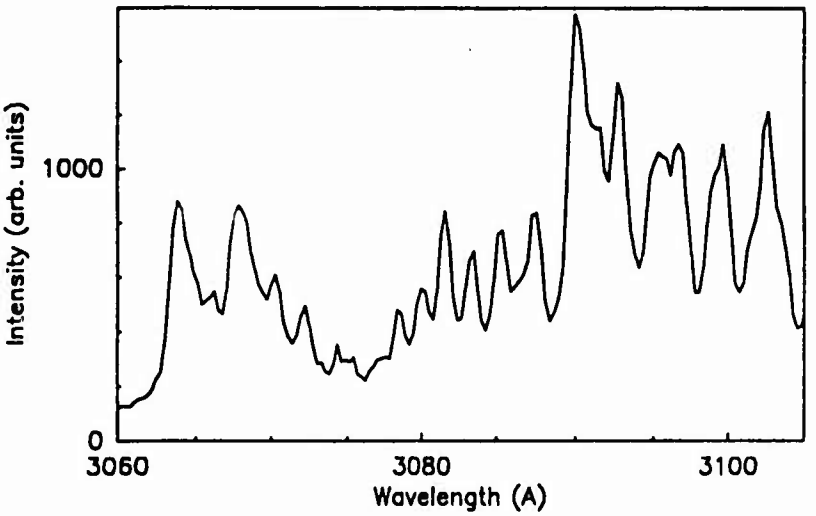

Figure 17. Emission Intensity as a Function of Wavelength for OH in HMX1 Burning in 1.5 MPa Nitrogen

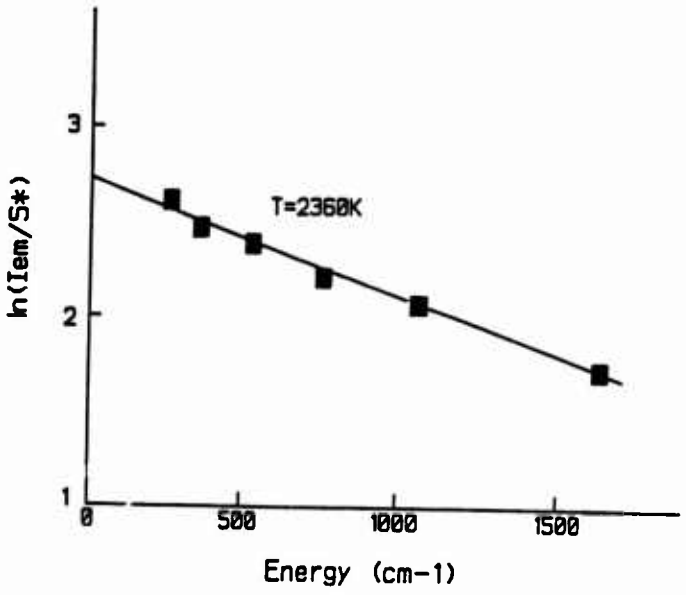

Figure 18. A Boltzmann Plot of OH Emission from a CH_4/N_2O Flame

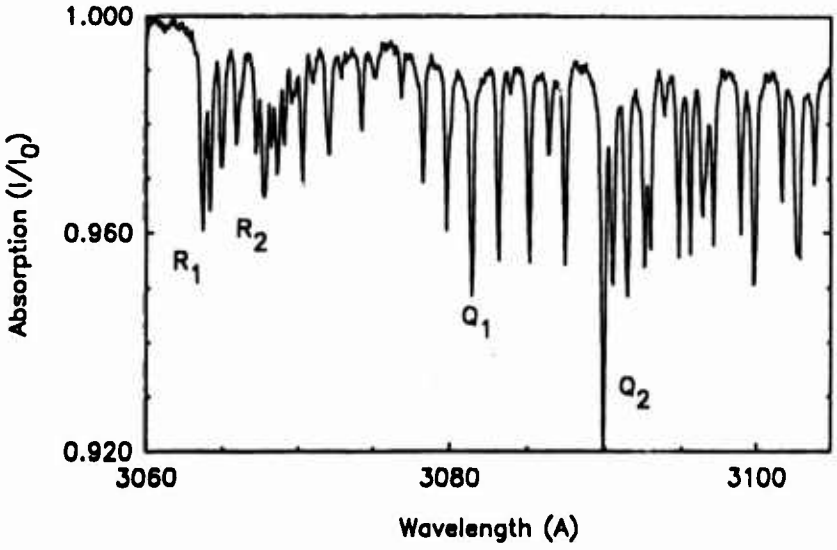

Figure 19. Absorption as a Function of Wavelength for OH in a CH_4/N_2O Flame

C. Absorption

Quantitative combustion diagnostic information can result from absorption measurements since they directly probe the ground state populations. Both temperature and concentrations can be obtained from absorption spectra, an example of which is displayed on Figure 19. Figure 19 represents an OH absorption spectrum taken for the atmospheric pressure CH_4/N_2O flame. The same rotational transitions as used for emission were used to generate a plot of ln $(I_{abs}/S_{J"J'\nu}C_2)$ versus $F_{J"}$ which is displayed on Figure 20. The resulting rotational ground state temperature ($T_{R"}$) was determined to be 2304 K ±190 K. Of the spectroscopic techniques reported here, these

rotational ground state temperatures are the closest approximation of translational temperatures, and in most cases are the same.

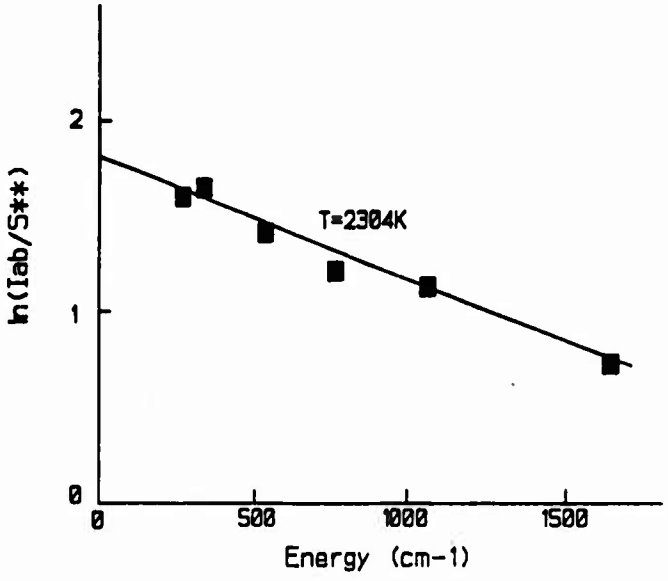

Figure 20. A Boltzmann Plot of OH Absorption from a CH_4/N_2O Flame

Summarizing the temperature information obtained from the three combustion systems studied the following has been observed. The best data, as one would expect, comes from the steady-state CH_4/N_2O flame calibration system. Here rotational emission and absorption spectra of OH and vibrational emission spectra of NH are all in excellent agreement. The rotational ground state temperature of $T_{R''} = 2304$ K is taken as the best representation of the temperature. At moderate resolution, the signal-to-noise ratio was insufficent to extract meaningful temperatures from the spectral data for either propellant. Although the concentrations that were computed from absorption spectra do not depend strongly on temperature over the range 1400 K to 2600 K (see Figure 21), a rough temperature profile is required in order to generate a concentration profile. Such a profile can be constructed from available data found mainly in the literature. Surface temperatures for burning composite propellants similar to those studied here are taken to be in the neighborhood of 600 K.[8,9-11,39] The final flame temperatures at constant pressure can be calculated by a thermochemical equilibrium code[24] (see Table 1). Moreover, support for these equilibrium temperatures comes from some experimental data. Stufflebeam and Eckbreth[23] have used CARS to measure temperatures as high as 2600 K in an HMX1 propellant burning in 2.3 MPa helium. Only a blackbody radiation estimate is available for the flame temperature of M-30, however, the value of 2587 K[1] is within a standard deviation of the equilibrium value. These temperature values fix the limits; it now remains to connect these limits. Taking into account some temperature-distance data of Kubota[39] and preliminary thermocouple measurements[40] on M-30 in 1.0 MPa nitrogen, rough temperature profiles that have been applied to the present data of both M-30 and HMX1 are shown on Figure 22. Here the surface temperature is taken as 600 K and the increase in temperature as a function of distance (to 0.5 mm) is shown as linear. At distances of 0.5 mm and greater, the temperature is constant at the equilibrium value.

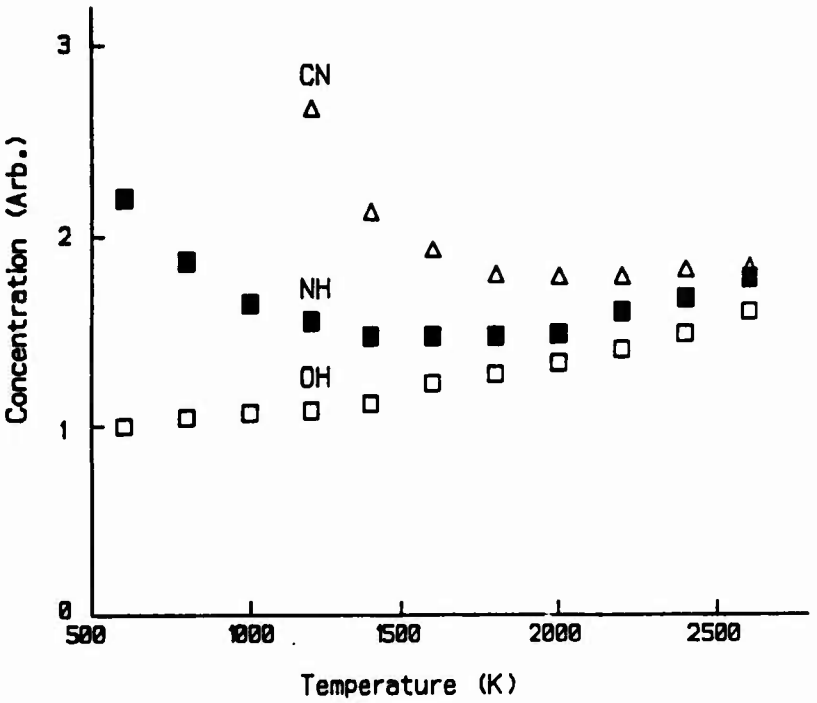

Figure 21. Temperature Dependence of the Computed Concentration for OH, NH, and CN When Using the Particular Sets of Transitions Described in the Text

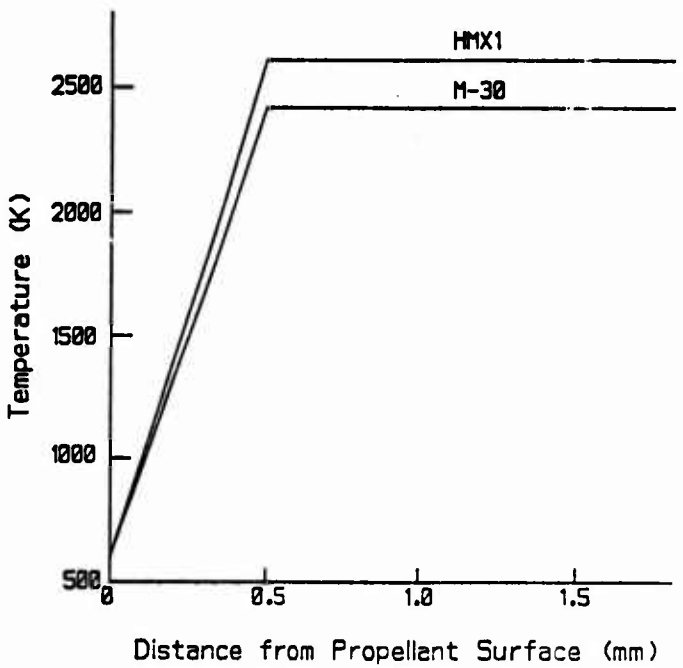

Figure 22. Constructed Temperature Profiles for HMX1 and M-30

Figure 19 is an example absorption spectrum from which absolute concentrations can be calculated through use of Eq. 4 if the temperature is known. In premixed laminar CH_4/N_2O flames, there is evidence[25,41] that the transient species concentrations peak about where the flame temperature reaches its equilibrium value and thus 2304 K has been used to compute the flame concentrations. The largest absorption observed in the well resolved OH spectrum is the Q_2 bandhead at 3089.8Å. Ten transitions within the spectral bandwidth of the monochromator contribute to this bandhead. They are given in Table 4 and included in performing the OH concentration calculations described here. The spectrometer slit function is taken as triangular with a FWHM of 0.033 nm and the molecular transitions are considered delta functions since their individual bandwidths are much less than the spectrometer or xenon arc lamp bandwidths. The computer program integrates over the spectrometer bandwidth and calculates an OH concentration from an experimental absorption value. A value of 2.35×10^{16} molecules/cc (7400 ppm) was calculated as a peak OH concentration for the atmospheric pressure CH_4/N_2O flame. A good example of OH spectra obtained for HMX1 propellant burning is shown on Figure 23. A comparison of Figures 19 and 23 dramatically illustrates one of the disadvantages present when gathering transient burning data. The CH_4/N_2O flame is steady state and thus the spectra can be leisurely improved by increasing the data gathering time. This is not the situation for a burning propellant; consequently the data of Figure 23 were obtained in a one second timeframe while the data of Figure 19 were obtained in a 200 second timeframe. The spectrum of Figure 23 has sufficient features to uniquely identify it as OH, but the signal-to-noise ratio was not sufficient to allow the spectral resolution displayed in Figure 19. Many spectra such as Figure 23, together with the temperature profiles of Figure 22, are used to generate absolute OH concentrations as a function of distance from the propellant surface. These profiles for M-30 burning in 1.0 MPa nitrogen and HMX1 burning in 1.5 MPa nitrogen are shown on Figure 24. In both cases, the OH concentration rises abruptly and then falls off much more slowly than either NH or CN (shown later). This general behavior is typical of many flame systems. The data indicate that HMX1 combustion has more OH present than does M-30. OH concentrations are plotted out to a distance of 5 mm above the propellant surface. At these distances, flame shape (coning) can reduce the absorption path length (see for example Figure 5). Significant differences between HMX1 and M-30 are shown in the video records of the propellant burns. At 5 mm from the propellant surface, the path length is approximately linearly reduced by 25% for HMX1 and a negligible amount for M-30. This path length correction has been accounted for in Figure 24 and the peak and equilibrium concentrations for HMX1 and M-30 are determined to be 1.6×10^{16} molecules/cc (380 ppm) and 4.5×10^{15} molecules/cc (150 ppm), respectively.

Absolute concentrations for NH have been determined from the 3360Å system absorption spectra (shown in emission on Figure 13). These spectra obtained for a CH_4/N_2O flame, M-30 and HMX1 are shown on Figures 25-27, respectively. The prominent feature is the (0,0) absorption bandhead occurring at 3360Å. Forty-eight transitions in this region were included to determine the NH concentration from the observed absorption. The flame spectrum is much better resolved than the propellant spectra. From the 1.6% absorption displayed on Figure 25, a value of 1.7×10^{14} molecules/cc (53 ppm) was computed for the absolute concentration of NH in an atmospheric pressure CH_4/N_2O flame. Absolute concentrations of NH as a function of distance from the propellant surface are shown for M-30 and HMX1 on Figures 28 and 29, respectively. These

Table 4. OH Rotational Transitions for Computing Concentrations from Spectral Absorptions

Transition	Wavelength
$Q_1(7)$	3089.73
$Q_1(7')$	3089.86
$Q_2(2)$	3089.86
$Q_2(2')$	3089.86
$Q_2(3)$	3089.86
$Q_2(3')$	3089.86
$Q_2(4')$	3090.27
$Q_2(4)$	3090.36
$Q_2(1')$	3090.45
$Q_2(1)$	3090.47

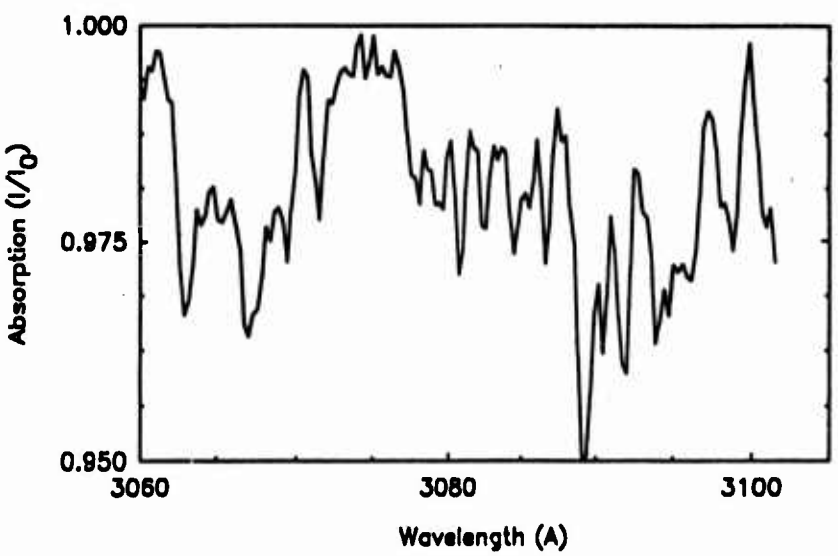

Figure 23. Absorption as a Function of Wavelength for OH in HMX1 Burning in 1.5 MPa Nitrogen

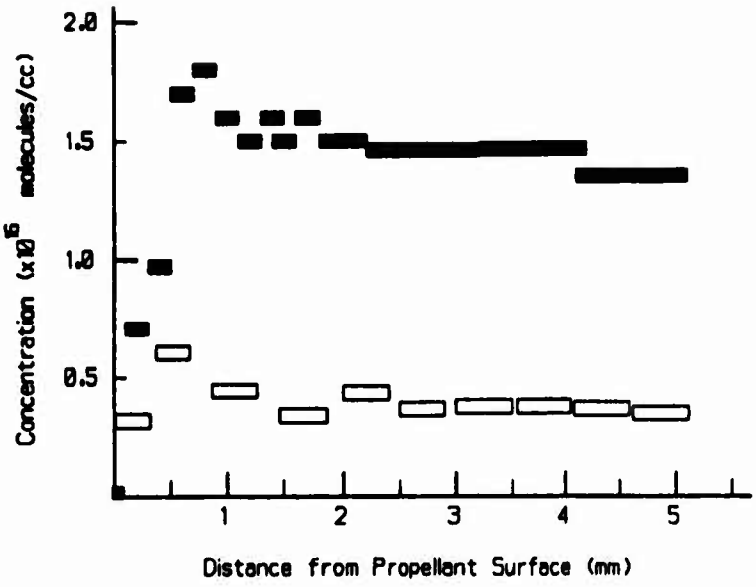

Figure 24. OH Concentration as a Function of Distance from the Propellant Surface for HMX1 at 1.5 MPa Nitrogen (▩) and M-30 at 1.0 MPa Nitrogen (□). The horizontal extent of the boxes represents the spatial extent over which the measurement was averaged.

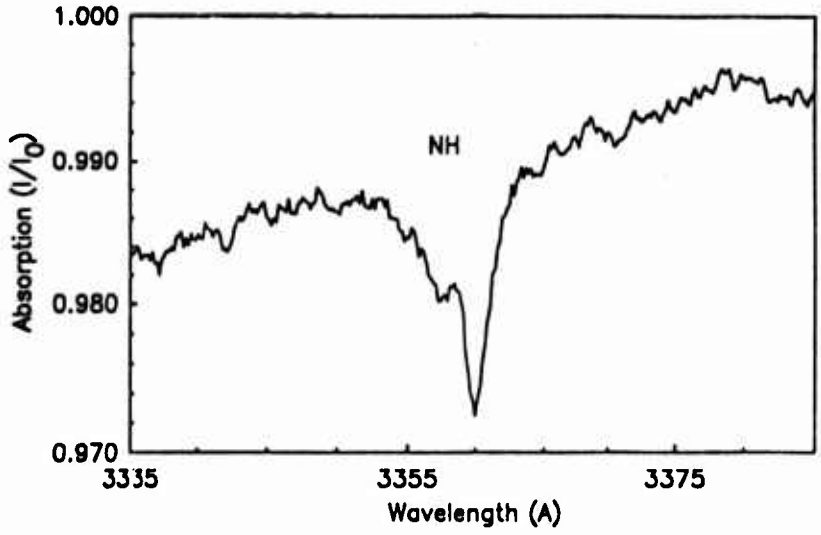

Figure 25. Absorption as a Function of Wavelength for NH in a CH_4/N_2O Flame

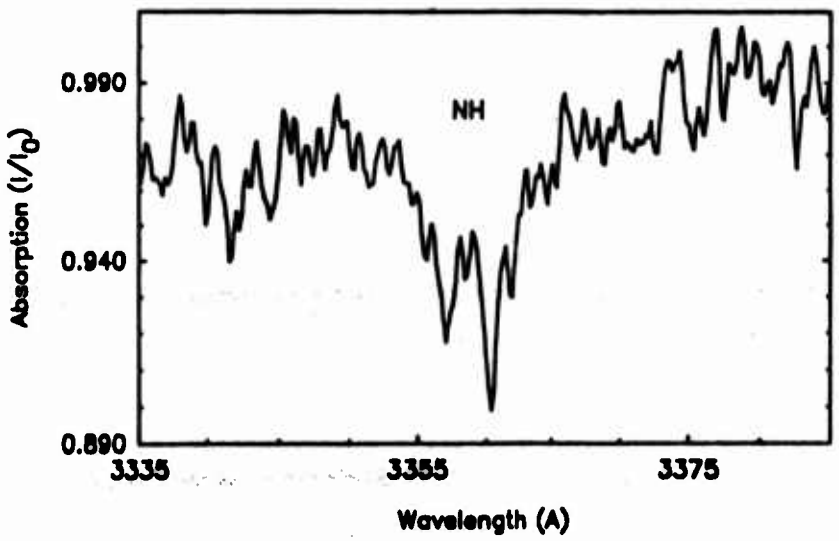

Figure 26. Absorption as a Function of Wavelength for NH in M-30 Burning in 1.0 MPa Nitrogen

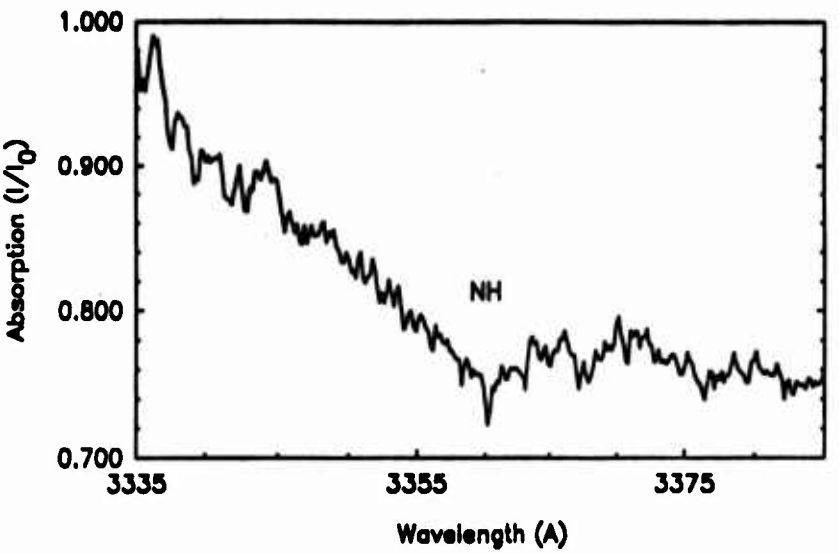

Figure 27. Absorption as a Function of Wavelength for NH in HMX1 Burning in 1.5 MPa Nitrogen

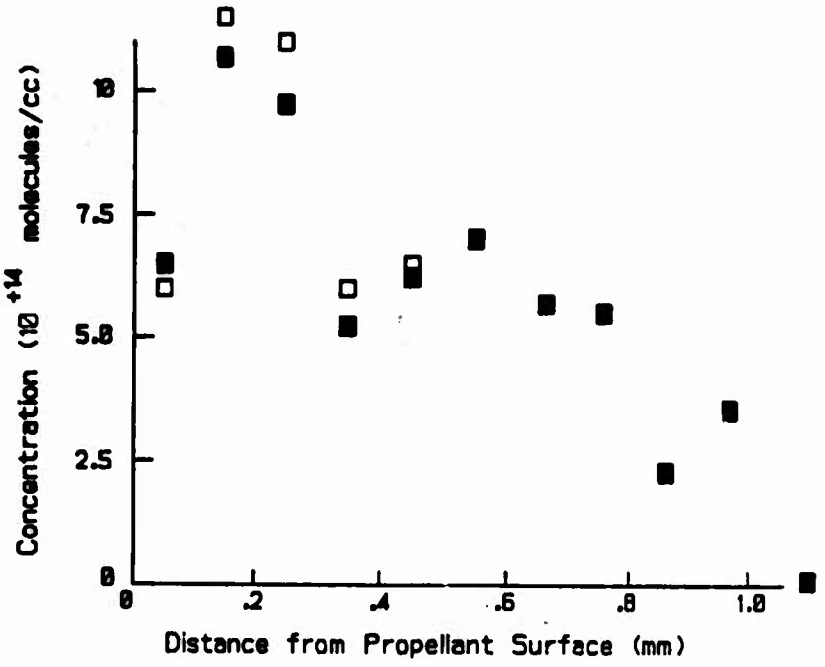

Figure 28. NH Concentration as a Function of Distance from the Propellant Surface for M-30 Burning in 1.0 MPa Nitrogen. The hatched squares are determined by using the constructed temperature profile. The open squares refer to concentration determinations using the adiabatic flame temperature.

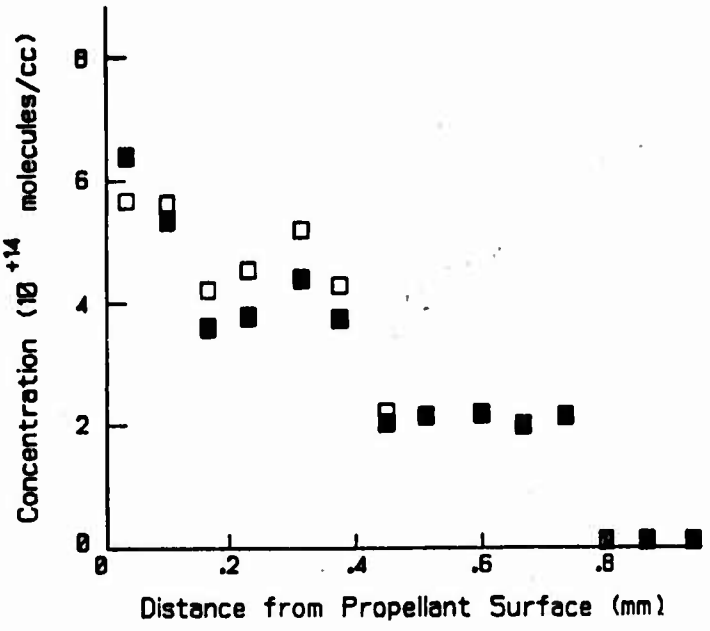

Figure 29. NH Concentration as a Function of Distance from the Propellant Surface for HMX1 Burning in 1.5 MPa Nitrogen. The squares have the same meaning as in Figure 28.

profiles have been generated from multiple spectra analogous to those of Figures 26 and 27. It is seen that NH is much more position sensitive than OH as the NH has disappeared at distances larger than about 1 mm from the propellant surface. Probable jitter of the flame front, together with the spatial resolution of the experiment, make it difficult to profile the build-up of the NH concentration in the HMX1 data, and here flame jitter can be observed from the video records. It has been demonstrated that there is a temperature dependence in the absorption calculations (Reference Figure 21), and thus, to explicitly show variation of the absolute concentration with temperature, the concentration values of Figures 28, 29, and 33 were plotted using two different temperature profiles, A and B. Temperature profile A is that of Figure 22 and is denoted with a dark square, while temperature profile B is a light square and represents an assumed constant temperature, the equilibrium flame temperature. At distances of about 0.2 mm and greater, these profiles merge. However the differences are not large at any point, indicating a low sensitivity of the results to the assumed temperature profile. Maximum values for NH in M-30 are about 1.1×10^{15} molecules/cc, however in terms of mole fraction there is 20 ppm NH with temperature profile A and 36 ppm NH with temperature profile B. Maximum NH values for HMX1, Figure 29, are not as obvious because there is no indication of increasing NH values. If 6×10^{14} molecules/cc is taken as the maximum value, then there are 5 ppm NH with temperature profile A and 14 ppm NH with temperature profile B. There appears to be an abrupt factor of two decrease in NH concentration around 0.4 mm from the propellant surface for both M-30 and HMX1. However, there is insufficient data to determine whether this feature is representative of the propellant flame profile or it comes about from path length variation caused by an unsteady flame front.

Absorptions from the violet system of CN have been used to obtain CN concentrations in the three combustion systems studied. Example absorption spectra for the CH_4/N_2O flame, M-30 and HMX1 are shown on Figures 30, 31, and 32, respectively. The prominent features, Figure 30, are the (0,0) and (1,1) absorptions at 3883.4Å and 3871.4Å, respectively. An accumulation time of 200 seconds was necessary to obtain the absorption of 0.7% at 3883.4Å shown on Figure 30. Sixty-four CN transitions from the (0,0) absorption bandhead were included in the calculation of the CN concentration and a value of 6.0×10^{13} molecules/cc (19 ppm) was obtained for the CH_4/N_2O flame. Only the (0,0) absorption feature is obvious for the noisier propellant spectra, and there was insufficient signal to generate an M-30 propellant CN concentration profile. The absorption spectrum shown on Figure 31 is taken as the peak CN concentration occurring around 0.2 mm above the propellant surface. The computed concentration using temperature profile A is 5.4×10^{14} molecules/cc (10 ppm) and 4.4×10^{14} molecules/cc (15 ppm) if temperature profile B is used. Three CN concentration profiles for HMX1 have been generated from absorption spectra similar to Figure 32. These profiles, obtained under identical conditions, are shown on Figures 33-35, where it can be seen that CN occurs over a short spatial extent of about 0.3 mm. A general reproducibility is observed in the data at distances greater than 0.1 mm where concentration values range from $2\text{-}3 \times 10^{14}$ molecules/cc at about 0.2 mm from the propellant surface. A large variation in CN concentration values at distances less than about 0.1 mm from the propellant surface is indicated on Figure 33. This divergence is due to the acute temperature sensitivity of this CN absorption at temperatures below 1500 K (see Figure 21). None of the CN profile data is sufficiently resolved to indicate a rise in CN concentration, thus a peak

value is uncertain. Nonetheless, with the present data for HMX1, a value of 5 x 10^{14} molecules/cc has been estimated which is similar to M-30.

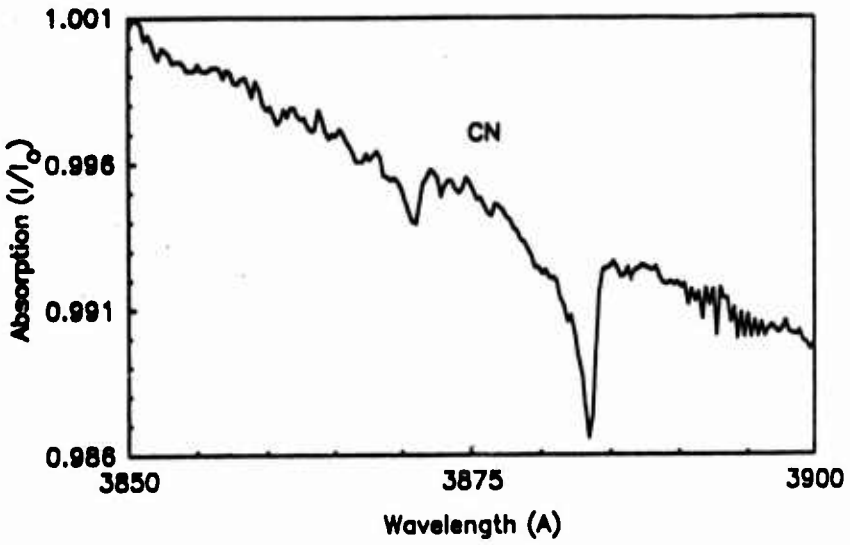

Figure 30. Absorption as a Function of Wavelength for CN in a CH_4/N_2O Flame

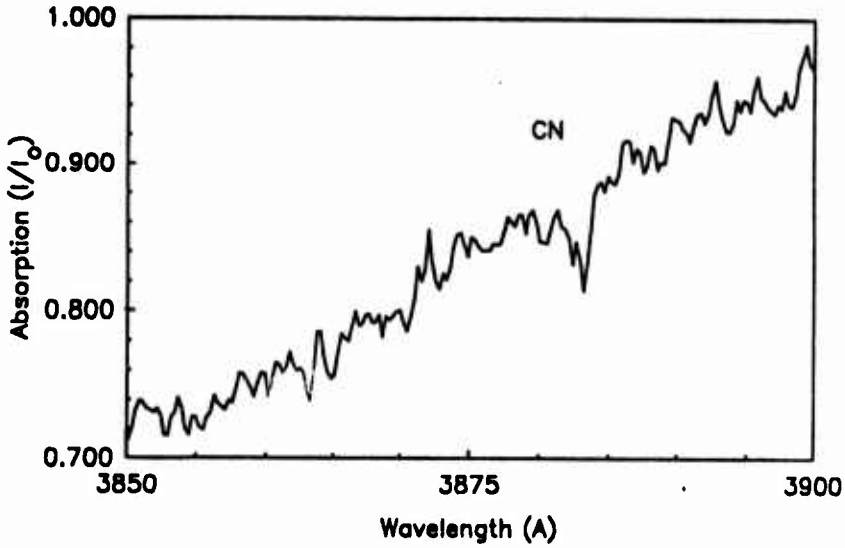

Figure 31. Absorption as a Function of Wavelength for CN in M-30 Burning in 1.0 MPa Nitrogen

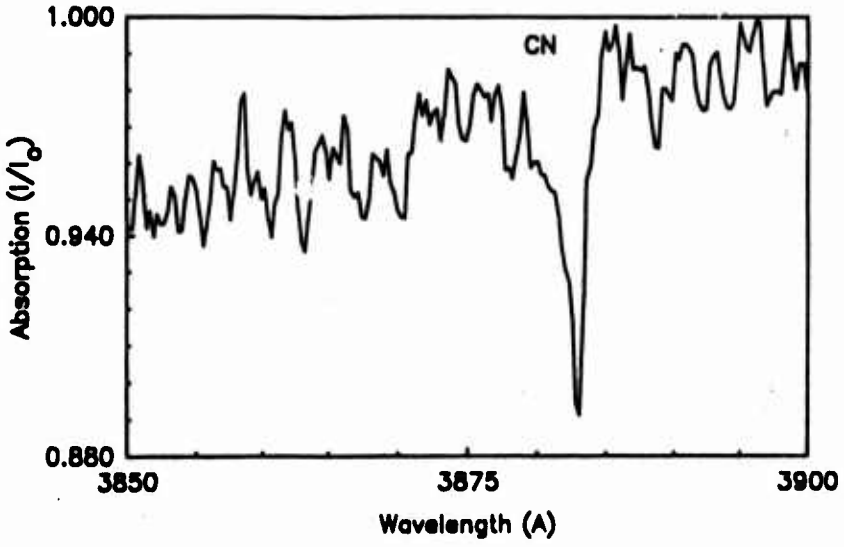

Figure 32. Absorption as a Function of Wavelength for CN in HMX1 Burning in 1.5 MPa Nitrogen

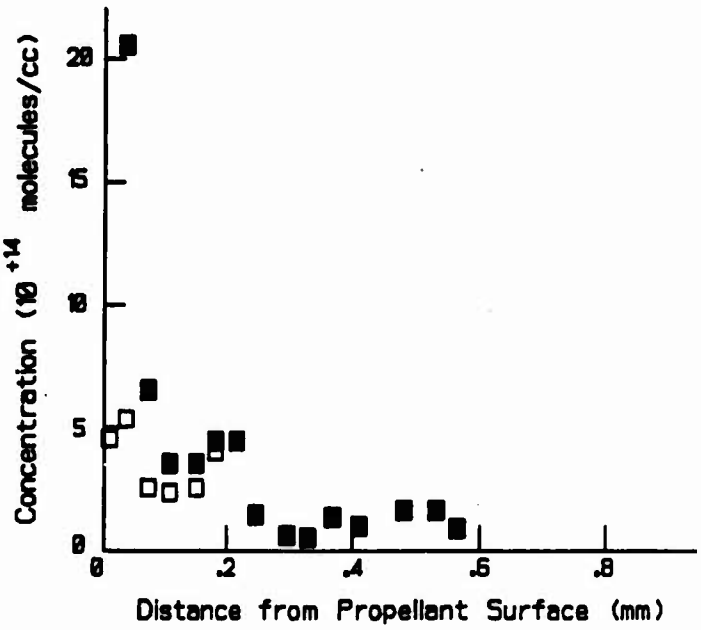

Figure 33. CN Concentration as a Function of Distance from the Propellant Surface for HMX1 Burning in 1.5 MPa Nitrogen. The squares have the same meaning as in Figure 28.

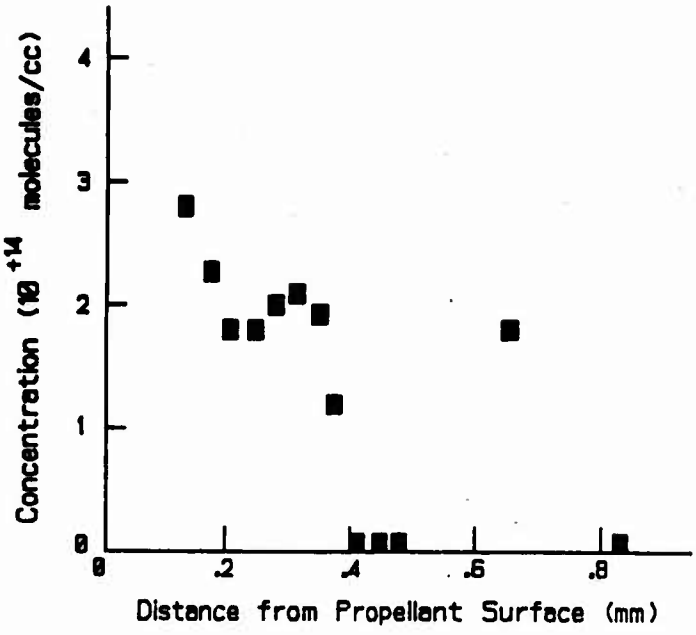

Figure 34. Same Conditions as Figure 33

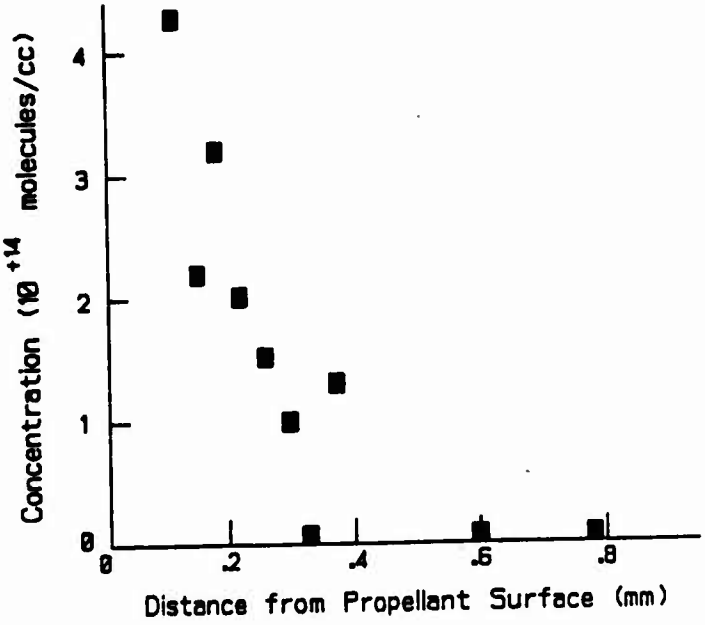

Figure 35. Same Conditions as Figure 33

VI. DISCUSSION AND SUMMARY

One of the combustion systems studied was a premixed laminar CH_4/N_2O flame burning in atmospheric pressure air. The primary purpose for probing this flame was to generate high quality, well understood spectra which would provide guidelines for interpreting the much noisier propellant spectra. The CH_4/N_2O flame has also been used to demonstrate various spectral techniques for obtaining a flame temperature. Here it was found that the emission spectroscopy of CN indicated abnormally high temperatures. This example points out that information from excited state species should be interpreted with caution. A realistic flame temperature was determined from a rotational analysis of ground state OH spectra. This temperature was then used, for example, in the computations of absolute concentrations of OH, NH, and CN occurring in the CH_4/N_2O flame. These data, however, should not be cited as quantitative for two reasons. First, the stoichiometry has not been monitored and small changes in this parameter can result in substantial concentration changes. Second, the absorption path length is too small (i.e., the edge effects may not be negligible) for serious consideration when performing quantitative absorption measurements on premixed laminar flames.

Experimental difference can be seen when comparing the emission and absorption data for the HMX1 propellant combustion system. It was determined that the emission intensities for NH and CN both peak around 0.6 mm from the propellant surface. If the position of peak emission intensity is interpreted also as the position of maximum concentration, then the concentrations derived from the absorption data, Figures 29, 33-35, are at odds with the emission results. The absorption results indicate that the peak concentrations of NH and CN are closer to the propellant surface than indicated by emission experiments. These results should be more reliable because the spatial resolution for absorption is defined by a collimated light beam whereas for emission[1] it is defined by collection optics. Consequently, for fluctuations in the propellant burning, the spatial resolution defined by a collection optic could be more susceptible to degradation.

Absolute concentrations for OH, NH, and CN are reported in Table 5 for two propellant combustion systems: HMX1 and M-30. No other experimental data or detailed chemical model has been found for a direct comparison for these, or any similar, propellants. OH is discussed first since the experimental spatial resolution seems adequate to observe general features of the OH concentration profiles. Moreover, equilibrium concentrations can be computed for OH and they are included in Table 5. These OH equilibrium concentrations are higher than the experimentally determined concentrations for both HMX1 and M-30. This means that the OH is not in equilibrium and/or the propellant gas temperature is below adiabatic. If OH is not in equilibrium, higher concentrations are expected since OH always overshoot for this type of flame system. Agreement can be made to occur between the equilibrium and experimental OH values by assuming that the propellant does not reach the adiabatic flame temperature. Both the equilibrium and experimental OH concentrations versus temperature are plotted for HMX1 and M-30 on Figures 36 and 37, respectively. The experimental curve was obtained by measuring the OH absorption occuring at about 1 mm from the propellant surface, and then computing the various concentrations that this absorption corresponded to assuming temperatures over the range of 2000 to 3000 K (the dashed line). The equilibrium OH concentration was obtained by starting with the propellant

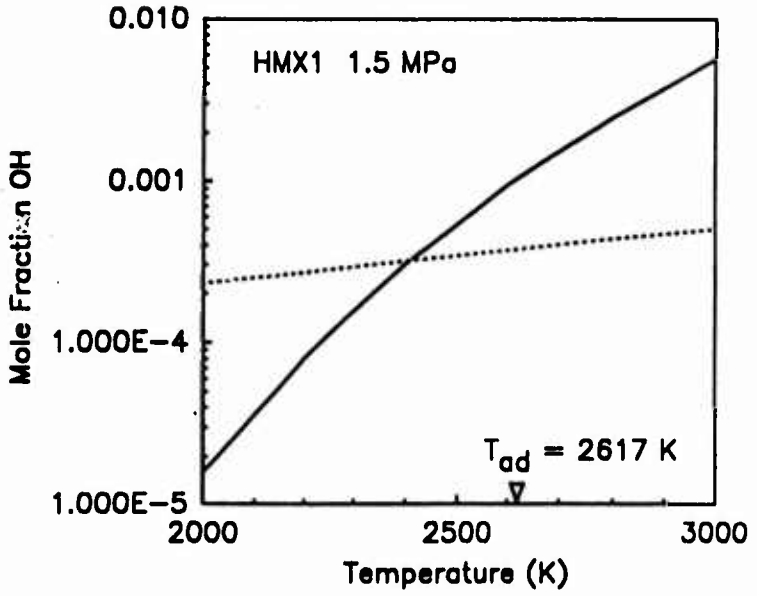

Figure 36. Computed Mole Fraction OH as a Function of Assumed Temperature for HMX1 Burning in 1.5 MPa Nitrogen. The solid line represents a thermochemical equilibrium calculation and the dashed line represents the temperature dependence of the experimental OH determination. The adiabatic flame temperature is 2617 K.

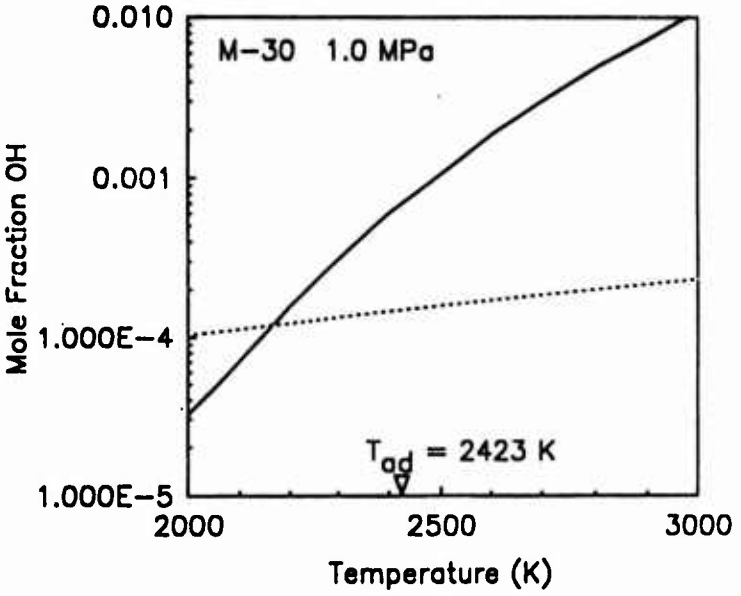

Figure 37. Computed Mole Fraction OH as a Function of Assumed Temperature for M-30 Burning in 1.0 MPa Nitrogen. The lines have the same meaning as in Figure 36. The adiabatic flame temperature is 2423 K.

ingredients and fixing the pressure to the experimental condition. The resulting curve as a function of temperature is shown as a solid line. It can be seen that the intersection of the curves on both Figures 36 and 37 fall below the adiabatic flame temperatures of 2617 K for HMX1 and 2430 K for M-30.

Table 5. Concentrations of OH, NH, and CN in M-30 and HMX1 Propellant Flames

System	T(K)	P(MPa)	OH(ppm)	NH(ppm)	CN(ppm)	Source
HMX1	2617	1.5	380	15*	12*	Present Work
HMX1	2617	1.5	1000			NASA-Lewis
HMX1	2420	1.5	305			NASA-Lewis
HMX1	2420	1.5	305			Present Work
M-30	2423	1.0	150	40	15*	Present Work
M-30	2423	1.0	680			NASA-Lewis
M-30	2170	1.0	120			NASA-Lewis
M-30	2170	1.0	120			Present Work

*Should not be considered maximum values.

There are several mechanisms which can contribute to this intersection occurring at less than the adiabatic flame temperature. Experimental uncertainty exists in the determination of the OH concentrations. The main contributors to this uncertainty are the signal-to-noise ratio of the data, the absorption path length, and the spectrometer resolution. A factor of 2 is the overall estimate for experimental error. Nonetheless, if it is assumed that the OH concentrations are a factor of 2 larger, the intersection for HMX1 is 2550 K and for M-30 is 2270 K, both of which are still less than the adiabatic values. Radiative losses from the gas and the burning surface are less than a 50 K correction. There are also conductive and convective heat losses at the edges where a nitrogen shroud gas is flowing. These losses have not been quantified, however, visual evidence of this effect can be seen on Figure 5b. Here the corners of the HMX1 propellant are not burning the same as the center portion of the propellant. It is conjectured that this is the dominant heat loss which is responsible for the propellant flame temperatures being about 200 K below the adiabatic values.

The transient chemical species, NH and CN, occur over a much smaller spatial extent than does OH. For this reason, effects such as non-horizontal burning and flame front fluctuations can be dramatic. In fact, there is enough scatter in the NH and CN data for HMX1 that the initial rise in concentration could not be determined. Hence, those concentrations reported in Table 5 should not be considered maximum values. Edwards[15] has performed laser induced fluorescence measurements on CN in HMX1 flames and reports a reaction zone thickness of about 0.4 mm. This result is consistent with the partial NH and CN profiles for HMX1 reported here. A better profile has been obtained for NH in M-30 where the initial rise in concentration is observed. A maximum concentration of 40 ppm is determined at a distance of about 0.2 mm from the propellant surface. The experimental uncertainty of this profile should be similar to that of OH; a factor of 2.

In summary, these concentration profiles of OH, NH, and CN are the first to be reported for a propellant flame environment. The OH concentration profiles provide evidence that the propellant flame has heat loss which yields a flame temperature about 200 K below adiabatic. The NH and CN species are very position sensitive, and thus, the spatial resolution of these profiles is poor. The biggest contributor to poor spatial resolution is from fluctuations of the flame front.

ACKNOWLEDGEMENTS

I express thanks to Dr. A.J. Kotlar for the computer programming to obtain species concentrations from absorption measurements, to Mr. S. Bunte for performing thermochemical equilibrium calculations, and to Dr. W.R. Anderson for discussions concerning the interpretation of some of the data.

INTENTIONALLY LEFT BLANK.

REFERENCES

1. J.A. Vanderhoff, "Spectral Studies of Propellant Combustion: Experimental Details and Emission Results for M-30 Propellant," BRL-MR-3714, Aberdeen Proving Ground, MD, December 1988.

2. J.A. Vanderhoff, "Spectral Emission and Absorption Studies of Solid Propellant Combustion," Proceedings, 25th JANNAF Combustion Meeting, Vol. IV, p. 537, 1988.

3. R.G. Rekers and D.S. Villars, "Flame Zone Spectroscopy of Solid Propellants," Rev. Sci. Instrum., Vol. 25(5) p. 424, 1954.

4. T. Edwards, D.P. Weaver, R. Adams, S. Hulsizer, and D.H. Campbell, "High-Pressure Combustor for the Spectroscopic Study of Solid Propellant Combustion Chemistry," Rev. Sci. Instrum., Vol. 56(11), p. 2131, 1985.

5. R.A. Fifer, "Chemistry of Nitrate Ester and Nitramine Propellants," in Fundamentals of Solid Propellant Combustion, edited by K. Kuo and M. Summerfield, AIAA Progress in Astronautics and Aeronautics Series, Vol. 90, 1984.

6. G. Lengelle, A. Bizot, J. Duterque, and J.F. Trubert, "Steady-State Burning of Homogeneous Propellants," in Fundamentals of Solid Propellant Combustion, edited by K. Kuo and M. Summerfield, AIAA Progress in Astronautics and Aeronautics Series, Vol. 90, 1984.

7. J.W. Glass and J.O.L. Wendt, "Mechanisms Governing the Destruction of Nitrogeneous Species During the Fuel Rich Combustion of Pulverized Coal," 19th Symposium (International) on Combustion, p. 1243, 1982.

8. N. Kubota, "Survey of Rocket Propellants and Their Combustion Characteristics," in Fundamentals of Solid Propellant Combustion, edited by K. Kuo and M. Summerfield, AIAA Progress in Astronautics and Aeronautics Series, Vol. 90, 1984.

9. R.L. Hatch, "Chemical Kinetics Modeling of HMX Combustion," Proceedings, 24th JANNAF Combustion Meeting, CPIA Publication 476, Vol. I, p. 383, 1987.

10. C.F. Melius, "Theoretical Studies of the Chemical Reactions Involved in the Ignition of Nitramines," Proceedings, 24th JANNAF Combustion Meeting, CPIA Publication 476, Vol. I, p. 359, 1987.

11. C.F. Melius, "The Gas-Phase Flame Chemistry of Nitramine Combustion," Proceedings, 25th JANNAF Combustion Meeting, CPIA Publication 498, Vol. II, p. 155, 1988.

12. N.E. Ermolin, O.P. Korobeinichev, L.V. Kuibida, and V.M. Fomin, Fiz. Goreniya Vzryva, Vol. 22, p. 54, 1986, and data presented therein by OP.O. Korobeinichev, et al., in Mass Spectrometry and Chemical Kinetics, Moscow, 1984.

13. G.A. Heath and R. Hirst, "Some Characteristics of the High Pressure Combustion of Double-Base Propellant," 8th Symposium (International) on Combustion, p. 711, 1962.

14. R.G. Rekers and D.S. Villars, "Flame Zone Spectroscopy of Solid Propellants. II. Double Base Propellant JPN*," J. Opt. Soc. Amer., Vol. 46(9), p. 534, 1956.

15. T. Edwards, "Solid Propellant Flame Spectroscopy," AFAL-TR-88-076, Edwards Air Force Base, CA, August 1988.

16. L.A Povinelli, "A Study of Composite Solid-Propellant Flame Structure Using a Spectral Radiation Shadowgraph Technique," AIAA Journal, Vol. 3(9), p. 1593, 1965.

17. R.H.W. Waesche, "Spectroscopic Studies of Solid Propellant Flames", Rohm and Haas Special Report S-111, Huntsville, AL, October 1966 (AD 376283).

18. V.M. Mal'tsev, A.G. Stasenko, V.A. Selezner, and P.F. Pokhil, "Spectroscopic Investigation of Combustion Zones of Flame Flares of Condensed Systems," Fizika Goreniya i Vzryva, Vol. 9(2), p. 220, 1973.

19. T. Edwards, D.P. Weaver, D.H. Campbell, and S. Hulsizer, "Investigation of High Pressure Solid Propellant Chemistry Using Emission Spectroscopy," J. Propulsion, Vol. 2(3), p. 228, 1986.

20. T. Edwards, D.P. Weaver, and D.H. Campbell, "Laser-Induced Fluorescence in High Pressure Solid Propellant Flames," Applied Optics, Vol. 26(17), p. 3496, 1987.

21. T. Parr and D.H. Parr, "Species and Temperature Profiles in Ignition and Deflagration of HMX," Western States Section/Combustion Institute, Paper WSS/CI 87-8, April 1987; and "Temperature Species Profiles in Propellant Ignition and Combustion," Proceedings, 24th JANNAF Combustion Meeting, CPIA Publication 476, Vol. I, pp. 367-382, 1987.

22. K. Aron and L.E. Harris, "CARS Probe of RDX Decomposition," Chem. Phys. Lett., Vol. 103(5), p. 413, 1984.

23. J.H. Stufflebeam and A.C. Eckbreth, "CARS Measurements of High Pressure Solid Propellant Combustion," Proceedings, 25th JANNAF Combustion Meeting, Vol. I, p. 113, 1988.

24. R.A. Svehla and B.J. McBride, "Fortran IV Computer Program for Calculation of Thermodynamic and Transport Properties of Complex Chemical Systems," NASA, TND-7056, 1973.

25. J.A. Vanderhoff, W.R. Anderson, A.J. Kotlar, and R.A. Beyer, "Raman and Fluorescence Spectroscopy in a Methane-Nitrous Oxide Laminar Flame," 20th Symposium (International) on Combustion, p. 1299, 1984.

26. K.P. Huber and G. Herzberg, Molecular Spectra and Molecular Structure. IV. Constants of Diatomic Molecules, Van Nostrand Reinhold Company, New York, 1979.

27. A.C. Eckbreth, P.A. Bonczyk, and J.A. Shirley, "Investigation of Saturated Laser Fluorescence and CARS Spectroscopic Techniques for Combustion Diagnostics," EPA-600/7-78-104, report on Contract No. 68-02-2176, United Technologies Research Center, East Hartford, CT, 1978.

28. R.P. Lucht, R.C. Peterson, and N.M. Laurendeau, "Fundamentals of Absorption Spectroscopy for Selected Diatomic Flame Radicals," PURDU-CL-78-06, report on NSF Grant ENG75-03461, Purdue University, West Lafayette, IN, 1978.

29. G. Herzberg, Molecular Spectra and Molecular Structure. I. Spectra of Diatomic Molecules, Van Nostrand Reinhold Company, New York, 1950.

30. A.C.G. Mitchell and M.W. Zemansky, Resonance Radiation and Excited Atoms, Cambridge University Press, New York, 1971.

31. W.L. Dimpfl and J.L. Kinsey, "Radiation Lifetimes of OH ($A^2\Sigma$) and Einstein Coefficients for the A-X System of OH and OD," J. Quant. Spec. Radiat. Transfer, Vol. 21, p. 233, 1979.

32. G. Dieke and H. Crosswhite, "The Ultraviolet Bands of OH: Fundamental Data," J. Quant. Spec. Radiat. Transfer, Vol. 2, p. 97, 1963.

33. N.L. Garland and D.R. Crosley, "Rotational Level Dependent Quenching of the $A^3\Pi_i$, v'=0 State of NH," J. Chem. Phys., Vol. 90(7), p. 3566, 1989.

34. P.W. Fairchild, G.P. Smith, D.R. Crosley, and J.J. Jeffries, "Lifetimes and Transition Probabilities for NH ($A^3\Pi_i$ - $X^3\Sigma^-$), Chem. Phys. Lett., Vol. 107, p. 181, 1984.

35. R.W. Nicholls, "Franck-Condon Factors to High Vibrational Quantum Numbers. III. CN," J. Res. Nat. Bur. Standards A, Vol. 68A, p. 75, 1964.

36. P.J. Knowles, H.J. Werner, P.J. Hay, and D.C. Cartwright, "The $A^2\Pi$ - $X^2\Sigma^+$ Red and $B^2\Sigma^+$ - $X^2\Sigma^+$ Violet Systems of the CN Radical: Accurate Multireference Configuration Interaction Calculations of the Radiative Transition Probabilities," J. Chem. Phys., Vol. 89, p. 7334, 1988.

37. M.S. Miller, unpublished data, Ballistic Research Laboratory, April 1988.

38. P. Guillaume and P.J. Van Tiggelen, "Spectroscopic Investigation of Acetylene-Nitrous Oxide Flames," 20th Symposium (International) on Combustion, p. 751, 1984, and references therein.

39. N. Kubota, "Physicochemical Processes of HMX Propellant Combustion," 9th Symposium (International) on Combustion, p. 777, 1982.

40. M.S. Miller, unpublished data, Ballistic Research Laboratory, May 1989.

41. W.R. Anderson, L.J. Decker, and A.J. Kotlar, "Temperature Profile of a Stoichiometric CH_4/N_2O Flame from Laser Excited Fluorescence Measurements on OH," Combustion and Flame, Vol. 48, p. 163, 1982.

INTENTIONALLY LEFT BLANK.

LIST OF ABBREVIATIONS, ACRONYMS, AND SYMBOLS

A	- Angstrom
AP	- Ammonium perchlorate
cc	- Cubic centimeter
cm	- Centimeter
E	- Energy (erg)
FWHM	- Full width half maximum
HMX	- Cyclotetramethylenetetranitramine
HMX1	- Nitramine propellant composed mainly of HMX
K	- Kelvin
LIF	- Laser induced fluorescence
m	- Meter
mm	- Millimeter
MPa	- Mega Pascal
ms	- Millisecond
M-30	- Triple base propellant composed mainly of nitroguanidine
NC	- Nitrocellulose
NG	- Nitroglycerin
nm	- Nanometer
NASA-Lewis	- Thermochemical equilibrium computer code
ppm	- Part per million
RDX	- Cyclotrimethylenetrinitramine
TMETN	- Trimethylolethanetrinitrate
T	- Temperature (K)
s	- Second
μm	- Micrometer
$A_{J',J''}$	- Einstein coefficient for spontaneous emission from level J' to level J" where $E_{J'} > E_{J''}$ (s^{-1})
$B_{J''J'}$	- Einstein coefficient for absorption in terms of spectral radiation energy densities ($cm^3/s^2 erg$)
$S_{J''J'}$	- Rotational line strength for a transition from J" to J'
$\nu_{J''J'}$	- Transition frequency for a transition from J" to J'
$q_{v''v'}$	- Franck-Condon factor
α_e, B_e, ω_e, $\omega_e\chi_e$	- Molecular constants for the equilibrium position
c	- Speed of light (cm/s)
C_1, C_2	- Constants

$F(J)$	- Rotational term energy for level J (cm^{-1})
$G(v)$	- Vibrational term energy for level v (cm^{-1})
g_e	- Electronic degeneracy
h	- Planck's constant (erg-s)
I_o	- Spectral intensity before entering absorbing medium ($erg/cm^2-cm^{-1}-s-steradian$)
I	- Spectral intensity after traversing path length L through the absorbing medium ($erg/cm^2-cm^{-1}-s-steradian$)
I_{em}	- Emission intensity
I_{abs}	- Absorption intensity
J	- Rotational quantum number
k	- Boltzmann constant (erg/k)
k_ν	- Spectral absorption coefficient (cm^{-1})
$\Delta\nu$	- Spectral slit width (cm^{-1})
L	- Path length (cm)
N_T	- Number density (cm^{-3})
Q_T	- Partition function
T	- Lifetime (s)

No of Copies	Organization
(Unclass., unlimited) 12	Administrator
(Unclass., limited) 2	Defense Technical Info Center
(Classified) 2	ATTN: DTIC-DDA
	Cameron Station
	Alexandria, VA 22304-6145
1	HQDA (SARD-TR)
	WASH DC 20310-0001
1	Commander
	US Army Materiel Command
	ATTN: AMCDRA-ST
	5001 Eisenhower Avenue
	Alexandria, VA 22333-0001
1	Commander
	US Army Laboratory Command
	ATTN: AMSLC-DL
	Adelphi, MD 20783-1145
2	Commander
	Armament RD&E Center
	US Army AMCCOM
	ATTN: SMCAR-MSI
	Picatinny Arsenal, NJ 07806-5000
2	Commander
	Armament RD&E Center
	US Army AMCCOM
	ATTN: SMCAR-TDC
	Picatinny Arsenal, NJ 07806-5000
1	Director
	Benet Weapons Laboratory
	Armament RD&E Center
	US Army AMCCOM
	ATTN: SMCAR-LCB-TL
	Watervliet, NY 12189-4050
1	Commander
	US Army Armament, Munitions
	and Chemical Command
	ATTN: SMCAR-ESP-L
	Rock Island, IL 61299-5000
1	Commander
	US Army Aviation Systems Command
	ATTN: AMSAV-DACL
	4300 Goodfellow Blvd.
	St. Louis, MO 63120-1798
1	Director
	US Army Aviation Research
	and Technology Activity
	Ames Research Center
	Moffett Field, CA 94035-1099

No of Copies	Organization
1	Commander
	US Army Missile Command
	ATTN: AMSMI-RD-CS-R (DOC)
	Redstone Arsenal, AL 35898-5010
1	Commander
	US Army Tank Automotive Command
	ATTN: AMSTA-TSL (Technical Library)
	Warren, MI 48397-5000
1	Director
	US Army TRADOC Analysis Command
	ATTN: ATAA-SL
	White Sands Missile Range, NM 88002-5
(Class. only) 1	Commandant
	US Army Infantry School
	ATTN: ATSH-CD (Security Mgr.)
	Fort Benning, GA 31905-5660
(Unclass. only) 1	Commandant
	US Army Infantry School
	ATTN: ATSH-CD-CSO-OR
	Fort Benning, GA 31905-5660
(Class. only) 1	The Rand Corporation
	P.O. Box 2138
	Santa Monica, CA 90401-2138
1	Air Force Armament Laboratory
	ATTN: AFATL/DLODL
	Eglin AFB, FL 32542-5000

Aberdeen Proving Ground

Dir, USAMSAA
ATTN: AMXSY-D
AMXSY-MP, H. Cohen

Cdr, USATECOM
ATTN: AMSTE-TO-F

Cdr, CRDEC, AMCCOM
ATTN: SMCCR-RSP-A
SMCCR-MU
SMCCR-MSI

Dir, VLAMO
ATTN: AMSLC-VL-D

DISTRIBUTION LIST

No. Of Copies	Organization
4	Commander US Army Research Office ATTN: R. Ghirardelli D. Mann R. Singleton R. Shaw P.O. Box 12211 Research Triangle Park, NC 27709-2211
2	Commander Armament R&D Center US Army AMCCOM ATTN: SMCAR-LCA-G, D.S. Downs J.A. Lannon Dover, NJ 07801
1	Commander Armament R&D Center US Army AMCCOM ATTN: SMCAR-LC-G, L. Harris Dover, NJ 07801
1	Commander Armament R&D Center US Army AMCCOM ATTN: SMCAR-SCA-T, L. Stiefel Dover, NJ 07801
2	Commander US Army Missile Command ATTN: AMSMI-RK, D.J. Ifshin W. Wharton Redstone Arsenal, AL 35898
1	Commander US Army Missile Command ATTN: AMSMI-RKA, A.R. Maykut Redstone Arsenal, AL 35898-5249
1	Office of Naval Research Department of the Navy ATTN: R.S. Miller, Code 432 800 N. Quincy Street Arlington, VA 22217
1	Commander Naval Air Systems Command ATTN: J. Ramnarace, AIR-54111C Washington, DC 20360
1	Commander Naval Surface Weapons Center ATTN: J.L. East, Jr., G-23 Dahlgren, VA 22448-5000
2	Commander Naval Surface Weapons Center ATTN: R. Bernecker, R-13 G.B. Wilmot, R-16 Silver Spring, MD 20902-5000
5	Commander Naval Research Laboratory ATTN: M.C. Lin J. McDonald E. Oran J. Shnur R.J. Doyle, Code 6110 Washington, DC 20375
1	Commanding Officer Naval Underwater Systems Center Weapons Dept. ATTN: R.S. Lazar/Code 36301 Newport, RI 02840
1	Commander Naval Weapons Center ATTN: T. Parr, Code 3895 Engineering Sciences Division China Lake, CA 93555-6001

DISTRIBUTION LIST

No. Of Copies	Organization
1	Superintendent Naval Postgraduate School Dept. of Aeronautics ATTN: D.W. Netzer Monterey, CA 93940
5	AFRPL/DY, Stop 24 ATTN: R. Corley R. Geisler J. Levine T. Edwards D. Weaver Edwards AFB, CA 93523-5000
1	AFRPL/MKPB, Stop 24 ATTN: B. Goshgarian Edwards AFB, CA 93523-5000
1	AFOSR ATTN: J.M. Tishkoff Bolling Air Force Base Washington, DC 20332
1	NASA Langley Research Center Langley Station ATTN: G.B. Northam/MS 168 Hampton, VA 23365
4	National Bureau of Standards ATTN: J. Hastie M. Jacox T. Kashiwagi H. Semerjian US Department of Commerce Washington, DC 20234
1	OSD/SDIO/UST ATTN: L.H. Caveny Pentagon Washington, DC 20301-7100
1	Aerojet Solid Propulsion Co. ATTN: P. Micheli Sacramento, CA 95813
1	Applied Combustion Technology, Inc. ATTN: A.M. Varney P.O. Box 17885 Orlando, FL 32860
2	Applied Mechanics Reviews The American Society of Mechanical Engineers ATTN: R.E. White A.B. Wenzel 345 E. 47th Street New York, NY 10017
1	Atlantic Research Corp. ATTN: M.K. King 5390 Cherokee Avenue Alexandria, VA 22314
1	Atlantic Research Corp. ATTN: R.H.W. Waesche 7511 Wellington Road Gainesville, VA 22065
1	AVCO Everett Rsch. Lab. Div. ATTN: D. Stickler 2385 Revere Beach Parkway Everett, MA 02149
1	Battelle Memorial Institute Tactical Technology Center ATTN: J. Huggins 505 King Avenue Columbus, OH 43201
1	Cohen Professional Services ATTN: N.S. Cohen 141 Channing Street Redlands, CA 92373
1	Exxon Research & Eng. Co. ATTN: A. Dean Route 22E Annandale, NJ 08801

DISTRIBUTION LIST

No. Of Copies	Organization
1	Ford Aerospace and Communications Corp. DIVAD Division Div. Hq., Irvine ATTN: D. Williams Main Street & Ford Road Newport Beach, CA 92663
1	General Applied Science Laboratories, Inc. 77 Raynor Avenue Ronkonkama, NY 11779-6649
1	General Electric Armament & Electrical Systems ATTN: M.J. Bulman Lakeside Avenue Burlington, VT 05401
1	General Electric Company 2352 Jade Lane Schenectady, NY 12309
1	General Electric Ordnance Systems ATTN: J. Mandzy 100 Plastics Avenue Pittsfield, MA 01203
2	General Motors Rsch Labs Physics Department ATTN: T. Sloan R. Teets Warren, MI 48090
2	Hercules, Inc. Allegany Ballistics Lab. ATTN: R.R. Miller E.A. Yount P.O. Box 210 Cumberland, MD 21501
1	Honeywell, Inc. Government and Aerospace Products ATTN: D.E. Broden/ MS MN50-2000 600 2nd Street NE Hopkins, MN 55343
1	Honeywell, Inc. ATTN: R.E. Tompkins MN38-3300 10400 Yellow Circle Drive Minnetonka, MN 55343
1	IBM Corporation ATTN: A.C. Tam Research Division 5600 Cottle Road San Jose, CA 95193
1	IIT Research Institute ATTN: R.F. Remaly 10 West 35th Street Chicago, IL 60616
2	Director Lawrence Livermore National Laboratory ATTN: C. Westbrook M. Costantino P.O. Box 808 Livermore, CA 94550
1	Lockheed Missiles & Space Co. ATTN: George Lo 3251 Hanover Street Dept. 52-35/B204/2 Palo Alto, CA 94304
1	Los Alamos National Lab ATTN: B. Nichols T7, MS-B284 P.O. Box 1663 Los Alamos, NM 87545
1	National Science Foundation ATTN: A.B. Harvey Washington, DC 20550
1	Olin Corporation Smokeless Powder Operations ATTN: V. McDonald P.O. Box 222 St. Marks, FL 32355

DISTRIBUTION LIST

No. Of Copies	Organization
1	Paul Gough Associates, Inc. ATTN: P.S. Gough 1048 South Street Portsmouth, NH 03801-5423
2	Princeton Combustion Research Laboratories, Inc. ATTN: M. Summerfield N.A. Messina 475 US Highway One Monmouth Junction, NJ 08852
1	Hughes Aircraft Company ATTN: T.E. Ward 8433 Fallbrook Avenue Canoga Park, CA 91303
1	Rockwell International Corp. Rocketdyne Division ATTN: J.E. Flanagan/HB02 6633 Canoga Avenue Canoga Park, CA 91304
4	Sandia National Laboratories Combustion Sciences Dept. ATTN: R. Cattolica S. Johnston C.F. Melius D. Stephenson Livermore, CA 94550
1	Science Applications, Inc. ATTN: R.B. Edelman 23146 Cumorah Crest Woodland Hills, CA 91364
1	Science Applications, Inc. ATTN: H.S. Pergament 1100 State Road, Bldg. N Princeton, NJ 08540
3	SRI International ATTN: G. Smith D. Crosley D. Golden 333 Ravenswood Avenue Menlo Park, CA 94025
1	Stevens Institute of Tech. Davidson Laboratory ATTN: R. McAlevy, III Hoboken, NJ 07030
1	Thiokol Corporation Elkton Division ATTN: W.N. Brundige P.O. Box 241 Elkton, MD 21921
1	Thiokol Corporation Huntsville Division ATTN: R. Glick Huntsville, AL 35807
4	Thiokol Corporation Wasatch Division ATTN: S.J. Bennett (3 copies) R.L. Hatch (1 copy) P.O. Box 524 Brigham City, UT 84302
2	United Technologies ATTN: A.C. Eckbreth J. Stufflebeam East Hartford, CT 06108
3	United Technologies Corp. Chemical Systems Division ATTN: R.S. Brown T.D. Myers (2 copies) P.O. Box 50015 San Jose, CA 95150-0015
1	Universal Propulsion Company ATTN: H.J. McSpadden Black Canyon Stage 1 Box 1140 Phoenix, AZ 85029
1	Veritay Technology, Inc. ATTN: E.B. Fisher 4845 Millersport Highway P.O. Box 305 East Amherst, NY 14051-0305

DISTRIBUTION LIST

No. Of Copies	Organization
1	Brigham Young University Dept. of Chemical Engineering ATTN: M.W. Beckstead Provo, UT 84601
1	California Institute of Tech. Jet Propulsion Laboratory ATTN: MS 125/159 4800 Oak Grove Drive Pasadena, CA 91103
1	California Institute of Technology ATTN: F.E.C. Culick/ MC 301-46 204 Karman Lab. Pasadena, CA 91125
1	University of California, Berkeley Mechanical Engineering Dept. ATTN: J. Daily Berkeley, CA 94720
1	University of California Los Alamos Scientific Lab. P.O. Box 1663, Mail Stop B216 Los Alamos, NM 87545
1	University of California, San Diego ATTN: F.A. Williams Dept. of Applied Mechanics & Engineering Sciences, B010 La Jolla, CA 92093
2	University of California, Santa Barbara Quantum Institute ATTN: K. Schofield M. Steinberg Santa Barbara, CA 93106
2	University of Southern California Dept. of Chemistry ATTN: S. Benson C. Wittig Los Angeles, CA 90007
1	Case Western Reserve Univ. Div. of Aerospace Sciences ATTN: J. Tien Cleveland, OH 44135
1	Cornell University Department of Chemistry ATTN: T.A. Cool Baker Laboratory Ithaca, NY 14853
1	Univ. of Dayton Rsch Inst. ATTN: D. Campbell AFRPL/PAP Stop 24 Edwards AFB, CA 93523
1	University of Delaware ATTN: T. Brill Chemistry Department Newark, DE 19711
1	University of Florida Dept. of Chemistry ATTN: J. Winefordner Gainesville, FL 32611
3	Georgia Institute of Technology School of Aerospace Engineering ATTN: E. Price W.C. Strahle B.T. Zinn Atlanta, GA 30332
1	University of Illinois Dept. of Mech. Eng. ATTN: H. Krier 144MEB, 1206 W. Green St. Urbana, IL 61801
1	Johns Hopkins University/APL Chemical Propulsion Information Agency ATTN: T.W. Christian Johns Hopkins Road Laurel, MD 20707

DISTRIBUTION LIST

No. Of Copies	Organization
1	University of Michigan Gas Dynamics Lab Aerospace Engineering Bldg. ATTN: G.M. Faeth Ann Arbor, MI 48109-2140
1	University of Minnesota Dept. of Mechanical Engineering ATTN: E. Fletcher Minneapolis, MN 55455
3	Pennsylvania State University Applied Research Laboratory ATTN: K.K. Kuo H. Palmer M. Micci University Park, PA 16802
1	Pennsylvania State University Dept. of Mechanical Engineering ATTN: V. Yang University Park, PA 16802
1	Polytechnic Institute of NY Graduate Center A S. Lederman 0 Farmingdale, NY 11735
2	Princeton University Forrestal Campus Library ATTN: K. Brezinsky I. Glassman P.O. Box 710 Princeton, NJ 08540
1	Purdue University School of Aeronautics and Astronautics ATTN: J.R. Osborn Grissom Hall West Lafayette, IN 47906
1	Purdue University Department of Chemistry ATTN: E. Grant West Lafayette, IN 47906
2	Purdue University School of Mechanical Engineering ATTN: N.M. Laurendeau S.N.B. Murthy TSPC Chaffee Hall West Lafayette, IN 47906
1	Rensselaer Polytechnic Inst. Dept. of Chemical Engineering ATTN: A. Fontijn Troy, NY 12181
1	Stanford University Dept. of Mechanical Engineering ATTN: R. Hanson Stanford, CA 94305
1	University of Texas Dept. of Chemistry ATTN: W. Gardiner Austin, TX 78712
1	University of Utah Dept. of Chemical Engineering ATTN: G. Flandro Salt Lake City, UT 84112
1	Virginia Polytechnic Institute and State University ATTN: J.A. Schetz Blacksburg, VA 24061
1	Commandant USAFAS ATTN: ATSF-TSM-CN Fort Sill, OK 73503-5600
1	F.J. Seiler Research Lab (AFSC) ATTN: S.A. Shakelford USAF Academy, CO 80840-6528
1	Freedman Associates ATTN: E. Freedman 2411 Diana Road Baltimore, MD 21209-1525

USER EVALUATION SHEET/CHANGE OF ADDRESS

This laboratory undertakes a continuing effort to improve the quality of the reports it publishes. Your comments/answers below will aid us in our efforts.

1. Does this report satisfy a need? (Comment on purpose, related project, or other area of interest for which the report will be used.) _____

2. How, specifically, is the report being used? (Information source, design data, procedure, source of ideas, etc.) _____

3. Has the information in this report led to any quantitative savings as far as man-hours or dollars saved, operating costs avoided, or efficiencies achieved, etc? If so, please elaborate. _____

4. General Comments. What do you think should be changed to improve future reports? (Indicate changes to organization, technical content, format, etc.) _____

BRL Report Number _____ Division Symbol _____

Check here if desire to be removed from distribution list. ____

Check here for address change. ____

Current address: Organization _____
Address _____

----------FOLD AND TAPE CLOSED----------

Director
U.S. Army Ballistic Research Laboratory
ATTN: SLCBR-DD-T
Aberdeen Proving Ground, MD 21005-5066

OFFICIAL BUSINESS

BUSINESS REPLY LABEL
FIRST CLASS PERMIT NO. 12062 WASHINGTON D.C.
POSTAGE WILL BE PAID BY DEPARTMENT OF THE ARMY

NO POSTAGE NECESSARY IF MAILED IN THE UNITED STATES

Director
U.S. Army Ballistic Research Laboratory
ATTN: SLCBR-DD-T
Aberdeen Proving Ground, MD 21005-9989